Phase-contrast magnetic resonance imaging and computational fluid dynamics assessment of thoracic aorta blood flow: a literature review

Omar A. Jarral, PhD[1], Matthew K. H. Tan, BSc[1], Yousuf Salmasi, MRCS[1], Selene Pirola, PhD[2], John R. Pepper, FRCS (CTh)[3], Declan P. O'Regan, PhD[4], Xiao Y. Xu, PhD[2], Thanos Athanasiou, PhD[1]

1. Department of Surgery and Cancer, Imperial College London, UK.
2. Department of Chemical Engineering, Imperial College London, UK.
3. National Heart and Lung Institute, Imperial College London, UK.
4. MRC London Institute of Medical Sciences, Imperial College London, UK.

Correspondence:

Dr. Omar A. Jarral, MBBS PhD MRCS (Eng)
Department of Surgery and Cancer,
Imperial College London,
Praed Street,
London,
W2 1NY.

Fax no.: +44 2085 632676
Tel no.: +44 7855 773118
Email: o.jarral@imperial.ac.uk

Word count: 6,609

VISUAL ABSTRACT

Key Question:
What is the role of MRI and computational fluid dynamics in the assessment and management of thoracic aortic disease?

Key Findings:
Both calculate complex variables, which relate to disease severity. Research is needed to validate clinical significance

Take-home Message:
Both are valuable techniques for assessing blood flow in the aorta, and will support the movement towards individualised patient management

ABSTRACT

The death rate from thoracic aortic disease is on the rise and represents a growing global health concern as patients are often asymptomatic before acute events which have devastating effects on health-related quality of life. Biomechanical factors have been found to play a major role in the development of both acquired and congenital aortic disease. Despite this, much is still unknown and translational benefits of this knowledge are yet to be seen. Phase-contrast cardiovascular magnetic resonance imaging (PC-CMR) of thoracic aortic blood flow has emerged as an exceptionally powerful non-invasive tool enabling visualisation of complex flow patterns, and calculation of variables such as wall-shear stress. This has led to multiple new findings in the areas of phenotype dependent bicuspid valve flow patterns, thoracic aortic aneurysm formation, and aortic prosthesis performance assessment. PC-CMR has also been used in conjunction with computational fluid modelling techniques to produce even more sophisticated analyses, by allowing the calculation of haemodynamic variables with exceptional temporal and spatial resolution. Translationally, these technologies may potentially play a major role in the emergence of precision medicine and patient-specific treatments in those with aortic disease. This clinically focused review will provide a systematic overview of key insights from published studies to date.

Key words: Magnetic Resonance Imaging, Phase-contrast MRI, Thoracic Aorta Disease

INTRODUCTION

The evolutionary development of the circulatory system in vertebrates has contributed significantly to the success of our species. It plays a key role in gas exchange, energy distribution, and excretion of waste products. The development of endothelium in our ancestors over half a billion years ago helped further optimise flow dynamics, barrier function, coagulation, and localised immune responses (1). Whilst circulatory system developments were driven by the time and distance constraints of diffusion, most evolutionary progress has been associated with trade-offs and limitations. Abnormal cardiovascular biomechanical forces have been implicated in many pathological conditions including atherosclerosis, aortic dissection, and bicuspid aortic valve (BAV) mediated aortic dilatation (2).

Scientific interest in studying these biomechanical factors has increased exponentially over the last fifty years. This has been enabled by rapid development of techniques in the following five areas: non-invasive imaging, endothelial cell biology, genomics, longitudinal clinical research, and multi-disciplinary approaches combining engineering with imaging and vascular biology. Whilst most developments have occurred in the 21st century, the link between flow and physiological function was hypothesised by great thinkers such as Leonardo Da Vinci in the 16th century, and Rudolf Virchow in the 19th century (3). Da Vinci famously postulated that the sinuses of Valsalva play a key role in creating retrograde flow and vortices that aid aortic valve (AV) closure and coronary perfusion in diastole (illustrated together with modern day imaging techniques in **Figure 1**). Virchow highlighted the spatial relationship between abnormal blood flow and atherosclerotic lesions, long before this was proven more substantially by the work of modern day scientists (4).

The focus of this review is on phase-contrast cardiovascular magnetic resonance imaging (PC-CMR) of the thoracic aorta. Techniques in this field are developing at an astounding pace, and have emerged as exceptionally powerful ways of assessing thoracic aortic blood flow for both scientists and clinicians. They are translationally relevant given the increasing burden and prevalence of "silent, but lethal" thoracic aortic disease (TAD), in both developed and developing nations (5). This clinical review focuses on all studies which assess thoracic aortic blood flow patterns with PC-CMR and related techniques such as computational fluid dynamics (CFD). Readers interested in the processes involved are directed to the included supplement which provides an overview of the workflows involved in PC-CMR and CFD analysis (**Supplement 1**).

METHODS

Medline and Google Scholar databases (up to January 2018) were used to search for clinically focused studies in English which assessed blood flow patterns in the thoracic aorta of adults using PC-CMR +/- CFD. The following search algorithm was used:

("4d mri" or "4d flow mri" or "time resolved 3d mri" or "2d mri" or "2d flow mri" or "phase contrast mri" or "computational modelling" or "flow sensitive mri" or "computational fluid dynamics") and ("thoracic aorta" or "ascending aorta" or "aortic root" or "aortic arch" or "descending thoracic aorta")

Reference lists of identified papers were also checked for additional studies. Studies were only included if they used patient specific boundary conditions. The following studies were excluded: studies published before the year 2000, those focusing purely on MRI and CFD technique methodology, those based on idealised (i.e. non-patient-specific) boundary conditions, repetitive studies from the same group, studies with less than 5 patients (MRI papers) or 2 simulations (CFD papers) with aortic pathology, and CT image-based studies.

Description of scientific terms used in papers

A number of scientific terms are used in papers which study flow in the aorta. A brief description is given of the key terms in order to help interpretation of the subsequent results:

Wall-shear stress (WSS): Within the aorta, there are two categories of stresses on the wall. Firstly, there is WSS due to the impact of blood flow immediately next to the vessel wall. The opposing force to this is friction, which is the force applied to blood from the aortic wall.

Secondly, there are circumferential, axial, and radial stresses on the vessel wall because of pulse pressure variation, generated by cyclical blood flow.

There are two key differences in these two categories of stress. Firstly, WSSs are applied to the superficial layer of the internal lumen of the aorta (i.e. the endothelium/intimal layers), whereas circumferential, axial, and radial stresses are transferred to all vessel wall layers. Secondly, WSS is significantly smaller in magnitude compared to circumferential stress. Despite this difference in magnitude, there has been significantly more research interest in WSS due to its role in altering endothelial cell biology, and the wide-ranging impact of this

Oscillatory-shear stress/index (OSI): OSI is a way of assessing the cyclic variation of WSS. It assesses how much the WSS vector deviates from its predominant axial direction of flow during one cardiac cycle. Its range is between 0 to 0.5, where a value of 0 indicates that WSS is directed in the primary direction of blood flow, and 0.5 indicates that the instantaneous vector of flow is never aligned with the overall time-averaged vector, indicating oscillatory behaviour.

Reynolds number: Turbulence of blood flow is often described with the Reynolds number (Re). This is a dimensionless parameter that describes viscous flows.

Helical flow: Helical flow is the cork-screw like flow of blood in the aorta.

Vortical flow: A region in blood where flow revolves around an axis line, which may be straight or curved.

RESULTS

A total of 83 studies are summarised in **(Supplement 2 - Tables S1-S6)**. These are categorised in to papers assessing blood flow patterns in healthy patients (7 studies), aortic valve disease (26 studies), thoracic aortic aneurysmal disease (14 studies), aortic coarctation (6 studies), aortic dissection (6 studies), and related to aortic prosthesis implantation (24 studies). If studies included multiple patient groups, they were categorised according to the size of the largest subgroup. A summary of the studies in each of these categories is given below.

Healthy patients

A total of seven studies were found which examined flow patterns in healthy patients of varying ages, all of which utilised 4D flow MRI **(Table S1)**, and none used CFD. Several typical and consistent findings were observed across age groups. Great segmental variation in patterns of wall-shear stress (WSS) were observed throughout the aorta, with the typical pattern showing a region of high WSS at the outer curve, and a region of low WSS (with high oscillatory shear index, OSI) at the inner curve of the ascending aorta (AA). The region of high WSS was seen to move to the outer curve of the arch, and inner curve of the descending aorta. Additionally, the atherogenic pattern of low WSS and high OSI was commonly observed at the origin of the head and neck vessels (6, 7). One group created population averaged reference maps of WSS, enabling the easy visualisation of patients who have abnormal segmental regions of WSS[7].

Helical flow was considered a normal finding in most volunteers, with the common pattern being right-handed in the AA, and left-handed in the descending thoracic aorta (DTA) (6, 8). Helical flow tended to appear in the AA following peak net forward flow, with more

coherence during the deceleration phase in the distal AA and proximal arch. There was little evidence of vortical flow in young patients, but this increased with age. This finding was consistent with the fact that the elderly demonstrated lower systolic, and higher retrograde velocities than the young (6, 9). **Figure 2** demonstrates the observation of two commonly described secondary flow patterns: helix and vortex formation.

One study examined the regional differences in flow instability, through calculation of the Reynolds number. Flow instability (based on critical Reynolds number defining instability) was seen in over half of healthy patients and observed more commonly in men. Instability was highest in the AA, followed by the DTA, and uncommonly seen in the arch (10). Only one study examined the influence of aortic geometry on flow patterns in the healthy, and surprisingly found it had less influence on flow patterns than age and aortic diameter (11). Finally, one study observed differences of flow velocity and velocity distribution in different age groups and between genders. There were significantly different peak velocities between age groups, and >40-year olds had greater velocity distribution than <21-year olds. Significant differences in all parameters were observed between men and women (12).

Aortic valve disease

Flow patterns secondary to aortic valve disease was the commonest studied area, with a total of twenty-six studies found, of which 3 used CFD (**Table S2)**. Most studies explored the influence of BAV, through comparisons with age and size matched controls. Peak and mean WSS was universally higher in patients with BAV (13-21). WSS patterns were also more circumferentially heterogeneous in this population in terms of position and magnitude (21-23). Authors often suggested that this was due to the BAV patients having a greater systolic flow angle, eccentric outflow jets and flow asymmetry due to restricted leaflet opening (14,

15, 18, 23-27). Characteristically, those with Right-Left BAV had distinct impinging jet flow patterns leading to regions of highest peak WSS on the right anterior aspect of the AA (16, 18, 19, 24, 28, 29). Those with Right-Non BAV had impingement and regions of highest WSS on the right and left posterior aspects of the AA (16, 18, 24, 29). The Right-Non-group was also associated with more severe flow abnormalities than Right-Left in three studies (14, 26, 27). **Figure 3** demonstrates the visualisation of blood flow in bicuspid patients compared to controls. A single novel study by Guzzardi et al. examined the relationship between WSS and tissue remodelling in BAV patients by assessing histology and protein expression in resected aortic specimens – regions of increased WSS corresponded with extracellular matrix dysregulation and elastic fibre degeneration (30).

BAV patients were also observed to have significantly greater abnormal helical flow, in terms of both quantity and magnitude (14-16, 21, 31, 32). This helical flow was often observed to be right-handed in the AA (similar to in the healthy), but more commonly seen to be left-handed in those with Right-Non valves (14, 16). Type 2 aortopathy was more prevalent in those with Right-Left, and Type 1/3 more common in those with Right-Non BAV (18, 19, 29). Several studies examined the influence of additional aortic valve disease on flow patterns in those with BAV. The addition of aortic stenosis or regurgitation tended to increase peak and mean WSS further (13, 14, 21, 26), as did aortic diameter (13, 22). In those with bicuspid regurgitant valves, WSS patterns tended to be universally elevated, whilst in those with bicuspid stenotic valves, WSS patterns had more eccentric patterns (19). A single study examined the influence of beta-blocker therapy in patients with BAV and found that WSS and peak velocity were not significantly different in the treatment group (13). Only two small studies longitudinally assessed the influence of flow patterns on long term outcomes

and found that both conjoint cusp opening angle and abnormal flow patterns predicted aortic growth at follow-up (23, 33).

A study by Allen et al. suggest that left ventricular abnormalities (hypertrophic obstructive cardiomyopathy) may also generate abnormal flow patterns and demonstrated that helical flow in the AA is significantly raised in those with basal-septal phenotype. The severity of changes was found to correlate with the outflow tract gradient and presence of systolic anterior motion of the mitral valve (34). A separate study by Schell et al. also suggested that aortic geometry (gothic and cubic arch) may influence the formation of vortex and helix formation (35). Interestingly, such helix and vortex inducing geometry was more common in first degree relatives (with TAV) of those with BAV.

Thoracic aortic aneurysmal disease

Fourteen studies examined flow patterns in patients with TAD (none of which used CFD), predominantly focusing on the proximal aorta **(Table S3)**. Two key patterns were observed in several studies:

Firstly, peak systolic WSS in the ascending aorta was lower in those with aneurysms and often seen to be inversely related to aortic size (36-38). Despite this, time averaged WSS was often higher than in controls due to a decreased systolic to diastolic WSS ratio, and delayed onset of peak WSS (36, 37). Maximal peak WSS was often observed on the anterior wall of the proximal aorta, and lowest on the proximal inner curve, and the right outer curve just before the arch (36-39). One study suggested that the addition of valvular disease increases WSS further (38). In patients with Marfan syndrome, eccentric WSS patterns were often observed, even in the absence of aneurysmal or valve disease. Marfan patients were also observed in two studies to have greater eccentricity of WSS patterns, which was highest at

252 the inner curve of the proximal aorta, and more anteriorly in its distal part (40, 41). Higher
253 OSI was observed at the STJ and in the arch, but lower in the DTA (40, 41).
254
255 Secondly, patients with proximal aortic aneurysms had significantly greater frequency of
256 helical and vortical flow. This was often related to aneurysm size, with appearance often
257 occurring earlier in the cardiac cycle in comparison to healthy controls (36, 37, 40, 42-44).
258 Given this, it was unsurprising to see that greater viscous energy loss and retrograde flow was
259 also observed in some studies (42, 45). In patients with Marfan syndrome, greater frequency
260 of helical and vortical flow was also observed, even in those without any evidence of
261 aneurysm or valve disease (40).
262
263 ***Aortic coarctation***
264 Six studies (of which four used CFD) examined flow patterns in patients pre- and post-
265 treatment for aortic coarctation **(Table S4)**. The majority of these suggested that patients
266 have the following differences compared to healthy individuals: greater evidence of helix and
267 vortex formation (especially in the proximal aorta, the head and neck vessels, and in the
268 region of the coarctation), greater turbulence, greater WSS magnitude in the proximal aorta,
269 and raised WSS or OSI in the region of the coarctation (46-50). Such changes were often
270 noted to be related to the degree of coarctation stenosis severity (50), and were often still
271 observed following coarctation repair (46, 47).
272
273 ***Aortic dissection***
274 Six studies (of which four used CFD) examined flow patterns in patients with mostly type B
275 dissection **(Table S5)**. They demonstrated that around the point of the primary entry tear,
276 there is often a region of increased velocity, WSS, pressure differential, and flow

abnormalities (51-53). Within the false lumen, slower velocities were observed, with more disturbed and complex flow patterns including vortex formation and systolic retrograde flow which occurred earlier than in the true lumen (53-55). Whilst these findings improved following stent treatment in two studies, flow abnormalities were often still present especially at the proximal end of the stent graft (52, 55).

Aortic prosthesis insertion

Twenty-four studies (of which seven used CFD) examined flow patterns following a range of mostly proximal aortic intervention **(Table S6)**. Several of these examined flow patterns in patients following aortic valve replacement (AVR) compared to healthy or pre-surgical controls. These studies demonstrated two key findings. Firstly, whilst post AVR patients often demonstrated less turbulent flow than pre-surgical controls (56), flow was often still eccentric when compared to healthy controls (57). Secondly, the choice of AVR prosthesis had a clear impact, with some studies suggesting that mechanical valves produce more vorticity, and bioprosthetic valves more helicity (57). The design of mechanical AVR's was reflected in their flow patterns – St. Jude mechanical prostheses demonstrated flow acceleration corresponding to jet orifices, and the development of reverse flow and vortices around the hinge housing (58, 59). Furthermore, one study used CFD to compare bioprosthetic and mechanical valves, showing higher WSS, transvalvular pressure drop, and turbulent kinetic energy with bioprostheses (60). One study suggested that more modern mechanical valve designs (On-X) produce more physiological flow patterns, more similar to that of healthy controls (61). Bioprostheses design also affected luminal velocity – higher central but lower outer lumen velocities were observed with stentless bioprostheses when compared to stented valves (62).

Several studies also compared flow patterns in patients following aortic root replacement, either with composite-valved prostheses (ARR), or valve-sparing root replacement (VSRR) (**Figure 4**). VSRR appeared to produce less asymmetry in flow, less helix formation, and superior haemodynamics when compared to ARR (59, 63-66). Despite this, both groups did not appear to be completely comparable to healthy controls, due to evidence of higher velocities, acceleration, jet formation, greater retrograde flow, and non-physiological helix and vortex formation (64, 66-72). The material properties of grafts clearly had an impact on flow patterns, as aortic geometry was often not normal following intervention, with evidence of energy loss and high levels of WSS at the distal anastomosis (63, 67) or distal to graft (73). One novel study examined the impact of implantation of a personalised external aortic support (PEARS) for Marfan syndrome. CFD analysis suggested that pre-operative high levels of peak stress present in the proximal aorta were transferred to the arch after implantation of the support, especially in the region of supported and unsupported aorta (74-76).

CONCLUSIONS

Our understanding behind the haemodynamic and biomechanical factors influencing aortic disease has increased exponentially over the last fifty years. PC-CMR and CFD have emerged as valuable non-invasive technologies for assessing aortic flow patterns in complex detail, both quantitatively and qualitatively. Based on the published literature, these technologies have led to three main benefits:

Firstly, it has led to several new findings which go beyond what scientists have learnt from other technologies such as Doppler ultrasound and hot film anemometry. Key advances have been made in the characterisation of phenotype dependent flow patterns in BAV, creation of population norm WSS maps, better descriptions of physiological and non-physiological helical flow patterns, and significantly more complex understanding behind the non-valvular factors influencing blood flow (e.g. LV outflow tract anatomy and aortic geometry). Comparative assessment of different aortic interventions (such as AVR, ARR, VSRR, and endovascular stent insertion) has highlighted prosthesis related factors which lead to both physiological and non-physiological blood flow.

Secondly, the colour visualisation of blood flow patterns has helped scientists and clinicians understanding of complex blood flow, which we believe has increased both creativity and interest from other disciplines and the public.

Thirdly, we believe that in the very near future these technologies will support precision medicine developments and allow patients with aortic disease to be treated on an individual basis guided by the variables such as WSS, peak wall stress, flow displacement and others.

Despite the above, most current MRI and CFD aortic research is only hypothesis generating. Most studies are cross-sectional and small to medium in size, without longitudinal follow-up. Before benefits can truly be reaped, further large population-based studies are required from which normalised population maps and ranges can be generated for the rich quantitative and qualitative variables produced. Based on this, longitudinal studies will be required to assess whether these variables are truly predictive of certain endpoints of interest. Correlation of these with patient reported outcome measures, and changes at an omics level has great potential to further develop this field. From a practical point of view, it is unclear how and which of these imaging technologies will transition in to the aortic clinic and multidisciplinary team meetings.

The limitations of these technologies must also be acknowledged. PC-CMR has limited temporal and spatial resolution. Several variables it produces are estimations, with accuracy dependent on acquisition parameters and multiple mathematical assumptions. The accuracy and reliability of WSS (which is estimated by near-wall velocity gradients) has been questioned given the challenges in vessel wall segmentation. Due to the low spatial resolution of MRI, blood flow velocities cannot be measured any closer to the aortic wall than 1000-1200 μm (affecting the calculation of velocity gradients), which is why the technique underestimates WSS. The temporal resolution of MRI also limits the ability to study the true dynamic and subtle nature of WSS patterns in animal vessels. Additionally, the technical quality of scans can be compromised by artefact from prostheses, and arrhythmias. CFD deals with some of these issues but comes at incredible computational cost. It also calculates variables based on multiple assumptions (e.g. it is often assumed that the aortic wall is rigid). Further technological advancements are required to address these limitations.

ABBREVIATIONS

AA, ascending aorta
CFD, computational fluid dynamics
DTA, descending thoracic aorta
MRI, magnetic resonance imaging
OSI, oscillatory shear index
PC-CMR, phase-contrast cardiovascular magnetic resonance imaging
TAD, thoracic aortic disease
WSS, wall-shear stress

SOURCES OF FUNDING

This work was jointly supported by the National Institute for Health Research (NIHR) Biomedical Research Centre (based at Imperial College London and Imperial College Healthcare NHS Trust), and the NIHR Cardiovascular Biomedical Research Unit (based at the Royal Brompton and Harefield NHS Foundation Trust). SP is supported by the H2020 EU Project MUSICARE—Multisectoral Integrative Approaches to Cardiac Care, Project ID MSCA-ITN 642458

DISCLOSURES

None

FIGURE LEGEND

Figure 1: A: velocity encoded images showing laminar flow through the aortic valve in a healthy male volunteer, B: Leonardo Da Vinci's illustration of vortices in the sinuses of Valsalva, C: Leonardo's highly accurate illustration of vortices in the aortic root, consistent with an image from modern day computational fluid dynamics techniques (from Bissell et al. (77), published by Oxford University Press (STM Signatory))

Figure 2: Secondary flow patterns with helicity seen in A and B and vortices depicted in C and D (from Frydrychowicz et al. 2012 (9), published by Springer Publishing Company (STM Signatory))

Figure 3: Visualisation of blood flow in bicuspid valves compared to controls (from Mahadevia et al. (18), published by Wolters Kluwer Health - Lippincott Williams & Wilkins (STM Signatory))

Figure 4: Visualisation of blood flow in VSRR (**A, B**) versus ARR (**C**) and controls (**D**) (from Collins et al. (68), published by Elsevier (STM Signatory))

REFERENCES

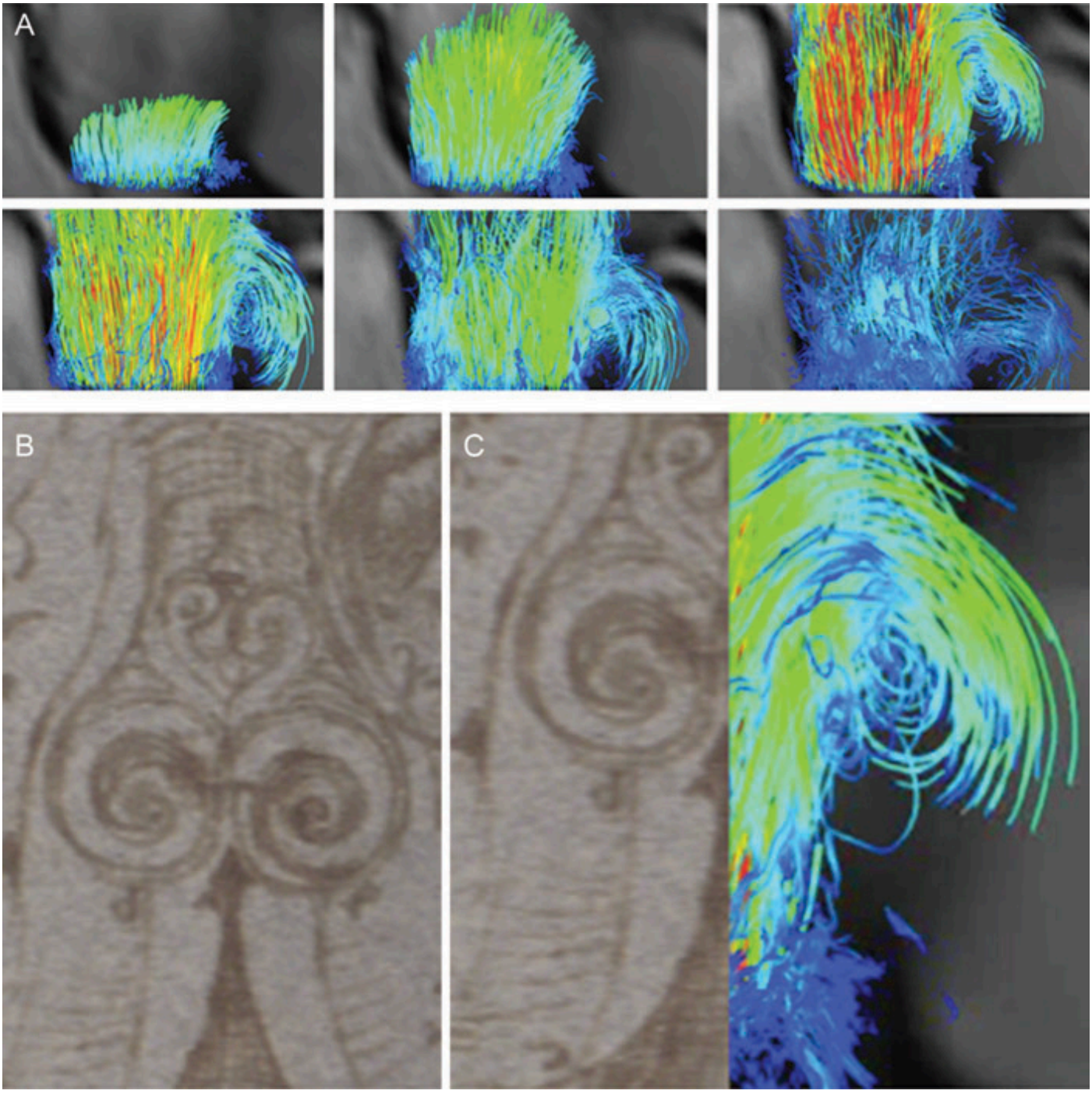
1. Monahan-Earley R, Dvorak AM and Aird WC. Evolutionary origins of the blood vascular system and endothelium. *J Thromb Haemost*. 2013;11 Suppl 1:46-66.
2. Back M, Gasser TC, Michel JB and Caligiuri G. Biomechanical factors in the biology of aortic wall and aortic valve diseases. *Cardiovasc Res*. 2013;99:232-41.
3. Evans PC and Kwak BR. Biomechanical factors in cardiovascular disease. *Cardiovasc Res*. 2013;99:229-31.
4. Friedman MH, Hutchins GM, Bargeron CB, Deters OJ and Mark FF. Correlation between intimal thickness and fluid shear in human arteries. *Atherosclerosis*. 1981;39:425-36.
5. Sampson UK, Norman PE, Fowkes FG, Aboyans V, Yanna S, Harrell FE, Jr. *et al*. Global and regional burden of aortic dissection and aneurysms: mortality trends in 21 world regions, 1990 to 2010. *Glob Heart*. 2014;9:171-180 e10.
6. Frydrychowicz A, Berger A, Russe MF, Stalder AF, Harloff A, Dittrich S *et al*. Time-resolved magnetic resonance angiography and flow-sensitive 4-dimensional magnetic resonance imaging at 3 Tesla for blood flow and wall shear stress analysis. *J Thorac Cardiovasc Surg*. 2008;136:400-7.
7. Frydrychowicz A, Stalder AF, Russe MF, Bock J, Bauer S, Harloff A *et al*. Three-dimensional analysis of segmental wall shear stress in the aorta by flow-sensitive four-dimensional-MRI. *J Magn Reson Imaging*. 2009;30:77-84.
8. Bogren HG, Buonocore MH and Valente RJ. Four-dimensional magnetic resonance velocity mapping of blood flow patterns in the aorta in patients with atherosclerotic coronary artery disease compared to age-matched normal subjects. *J Magn Reson Imaging*. 2004;19:417-27.
9. Frydrychowicz A, Berger A, Munoz Del Rio A, Russe MF, Bock J, Harloff A *et al*. Interdependencies of aortic arch secondary flow patterns, geometry, and age analysed by 4-dimensional phase contrast magnetic resonance imaging at 3 Tesla. *Eur Radiol*. 2012;22:1122-30.
10. Stalder AF, Frydrychowicz A, Russe MF, Korvink JG, Hennig J, Li K *et al*. Assessment of flow instabilities in the healthy aorta using flow-sensitive MRI. *J Magn Reson Imaging*. 2011;33:839-46.
11. Morbiducci U, Ponzini R, Rizzo G, Cadioli M, Esposito A, Montevecchi FM *et al*. Mechanistic insight into the physiological relevance of helical blood flow in the human aorta: an in vivo study. *Biomech Model Mechanobiol*. 2011;10:339-55.
12. Garcia J, van der Palen RLF, Bollache E, Jarvis K, Rose MJ, Barker AJ *et al*. Distribution of blood flow velocity in the normal aorta: Effect of age and gender. *J Magn Reson Imaging*. 2018;47:487-498.
13. Allen BD, Markl M, Barker AJ, van Ooij P, Carr JC, Malaisrie SC *et al*. Influence of beta-blocker therapy on aortic blood flow in patients with bicuspid aortic valve. *Int J Cardiovasc Imaging*. 2016;32:621-8.
14. Bissell MM, Hess AT, Biasiolli L, Glaze SJ, Loudon M, Pitcher A *et al*. Aortic dilation in bicuspid aortic valve disease: flow pattern is a major contributor and differs with valve fusion type. *Circ Cardiovasc Imaging*. 2013;6:499-507.
15. Faggiano E, Antiga L, Puppini G, Quarteroni A, Luciani GB and Vergara C. Helical flows and asymmetry of blood jet in dilated ascending aorta with normally functioning bicuspid valve. *Biomech Model Mechanobiol*. 2013;12:801-13.
16. Hope MD, Hope TA, Meadows AK, Ordovas KG, Urbania TH, Alley MT *et al*. Bicuspid aortic valve: four-dimensional MR evaluation of ascending aortic systolic flow patterns. *Radiology*. 2010;255:53-61.
17. Hope MD, Hope TA, Crook SE, Ordovas KG, Urbania TH, Alley MT *et al*. 4D flow CMR in assessment of valve-related ascending aortic disease. *JACC Cardiovasc Imaging*. 2011;4:781-7.

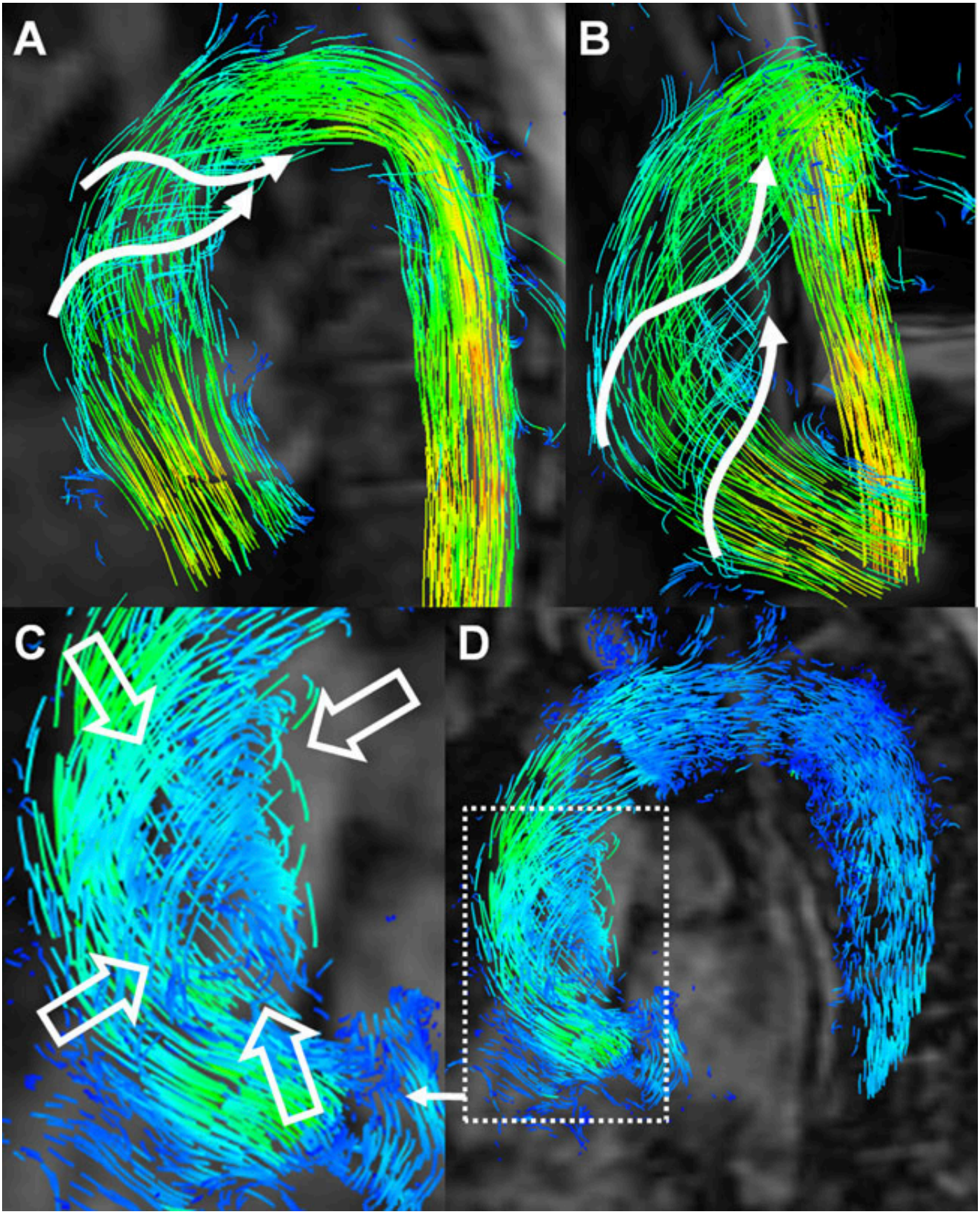
18. Mahadevia R, Barker AJ, Schnell S, Entezari P, Kansal P, Fedak PW *et al*. Bicuspid aortic cusp fusion morphology alters aortic three-dimensional outflow patterns, wall shear stress, and expression of aortopathy. *Circulation*. 2014;129:673-82.
19. Shan Y, Li J, Wang Y, Wu B, Barker AJ, Markl M *et al*. Aortic shear stress in patients with bicuspid aortic valve with stenosis and insufficiency. *J Thorac Cardiovasc Surg*. 2017.
20. van Ooij P, Potters WV, Collins J, Carr M, Carr J, Malaisrie SC et al. Characterization of abnormal wall shear stress using 4D flow MRI in human bicuspid aortopathy. *Ann Biomed Eng*. 2015;43:1385-97.
21. von Knobelsdorff-Brenkenhoff F, Karunaharamoorthy A, Trauzeddel RF, Barker AJ, Blaszczyk E, Markl M *et al*. Evaluation of Aortic Blood Flow and Wall Shear Stress in Aortic Stenosis and Its Association With Left Ventricular Remodeling. *Circ Cardiovasc Imaging*. 2016;9:e004038.
22. Barker AJ, Lanning C and Shandas R. Quantification of hemodynamic wall shear stress in patients with bicuspid aortic valve using phase-contrast MRI. *Ann Biomed Eng*. 2010;38:788-800.
23. Della Corte A, Bancone C, Conti CA, Votta E, Redaelli A, Del Viscovo L *et al*. Restricted cusp motion in right-left type of bicuspid aortic valves: a new risk marker for aortopathy. *J Thorac Cardiovasc Surg*. 2012;144:360-9, 369 e1.
24. Entezari P, Schnell S, Mahadevia R, Malaisrie C, McCarthy P, Mendelson M *et al*. From unicuspid to quadricuspid: influence of aortic valve morphology on aortic three-dimensional hemodynamics. *J Magn Reson Imaging*. 2014;40:1342-6.
25. Mirabella L, Barker AJ, Saikrishnan N, Coco ER, Mangiameli DJ, Markl M *et al*. MRI-based Protocol to Characterize the Relationship Between Bicuspid Aortic Valve Morphology and Hemodynamics. *Ann Biomed Eng*. 2015;43:1815-27.
26. Youssefi P, Gomez A, He T, Anderson L, Bunce N, Sharma R *et al*. Patient-specific computational fluid dynamics-assessment of aortic hemodynamics in a spectrum of aortic valve pathologies. *J Thorac Cardiovasc Surg*. 2017;153:8-20 e3.
27. Raghav V, Barker AJ, Mangiameli D, Mirabella L, Markl M and Yoganathan AP. Valve mediated hemodynamics and their association with distal ascending aortic diameter in bicuspid aortic valve subjects. *J Magn Reson Imaging*. 2018;47:246-254.
28. Barker AJ, Markl M, Burk J, Lorenz R, Bock J, Bauer S *et al*. Bicuspid aortic valve is associated with altered wall shear stress in the ascending aorta. *Circ Cardiovasc Imaging*. 2012;5:457-66.
29. Burris NS and Hope MD. Bicuspid valve-related aortic disease: flow assessment with conventional phase-contrast MRI. *Acad Radiol*. 2015;22:690-6.
30. Guzzardi DG, Barker AJ, van Ooij P, Malaisrie SC, Puthumana JJ, Belke DD *et al*. Valve-Related Hemodynamics Mediate Human Bicuspid Aortopathy: Insights From Wall Shear Stress Mapping. *J Am Coll Cardiol*. 2015;66:892-900.
31. Lorenz R, Bock J, Barker AJ, von Knobelsdorff-Brenkenhoff F, Wallis W, Korvink JG *et al*. 4D flow magnetic resonance imaging in bicuspid aortic valve disease demonstrates altered distribution of aortic blood flow helicity. *Magn Reson Med*. 2014;71:1542-53.
32. Garcia J, Barker AJ, Collins JD, Carr JC and Markl M. Volumetric quantification of absolute local normalized helicity in patients with bicuspid aortic valve and aortic dilatation. *Magn Reson Med*. 2017;78:689-701.
33. Hope MD, Wrenn J, Sigovan M, Foster E, Tseng EE and Saloner D. Imaging biomarkers of aortic disease: increased growth rates with eccentric systolic flow. *J Am Coll Cardiol*. 2012;60:356-7.
34. Allen BD, Choudhury L, Barker AJ, van Ooij P, Collins JD, Bonow RO *et al*. Three-dimensional haemodynamics in patients with obstructive and non-obstructive hypertrophic cardiomyopathy assessed by cardiac magnetic resonance. *Eur Heart J Cardiovasc Imaging*. 2015;16:29-36.

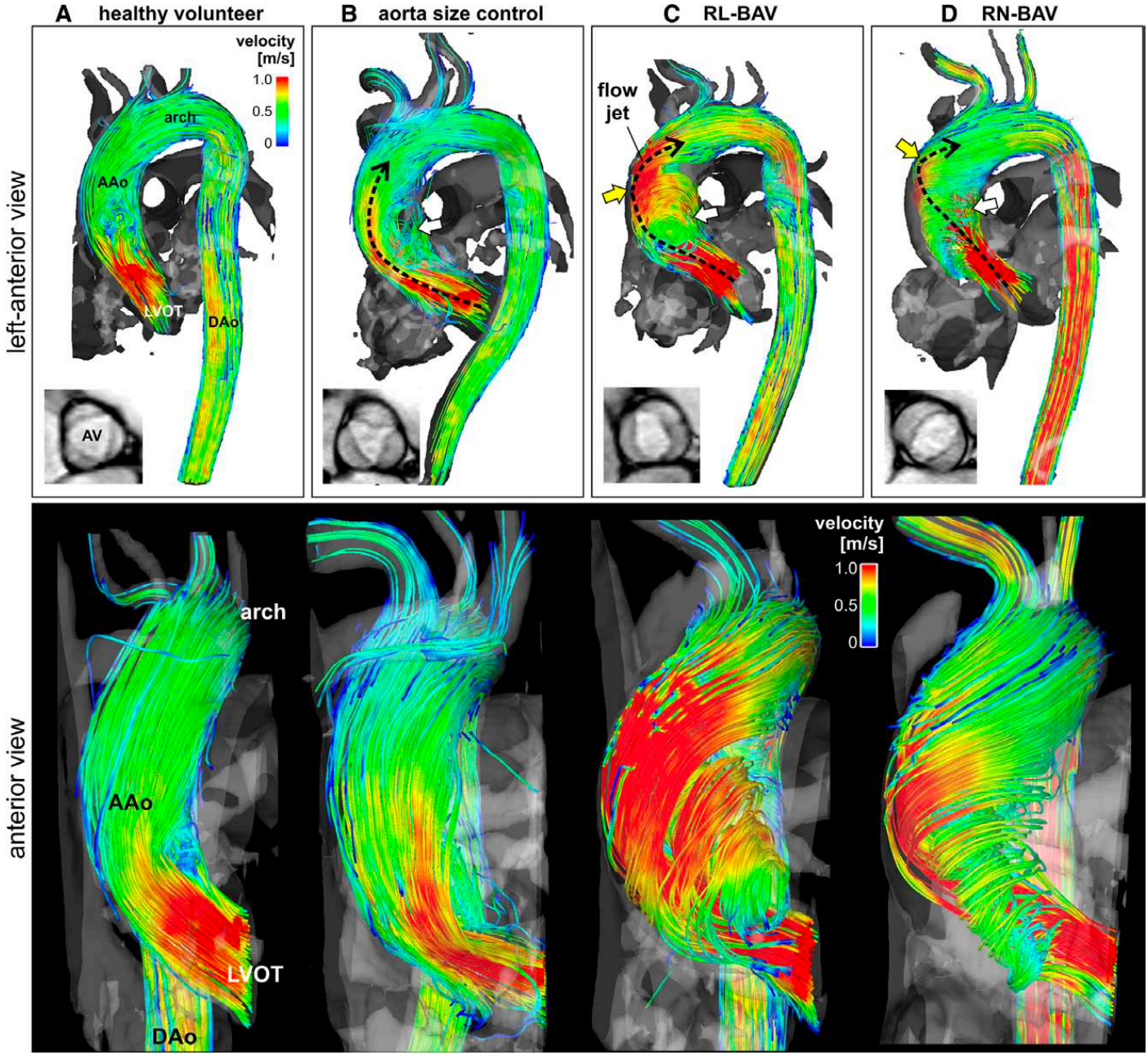
35. Schnell S, Smith DA, Barker AJ, Entezari P, Honarmand AR, Carr ML *et al*. Altered aortic shape in bicuspid aortic valve relatives influences blood flow patterns. *Eur Heart J Cardiovasc Imaging*. 2016;17:1239-1247.
36. Bieging ET, Frydrychowicz A, Wentland A, Landgraf BR, Johnson KM, Wieben *et al*. In vivo three-dimensional MR wall shear stress estimation in ascending aortic dilatation. *J Magn Reson Imaging*. 2011;33:589-97.
37. Burk J, Blanke P, Stankovic Z, Barker A, Russe M, Geiger J *et al*. Evaluation of 3D blood flow patterns and wall shear stress in the normal and dilated thoracic aorta using flow-sensitive 4D CMR. *J Cardiovasc Magn Reson*. 2012;14:84.
38. van Ooij P, Potters WV, Nederveen AJ, Allen BD, Collins J, Carr J *et al*. A methodology to detect abnormal relative wall shear stress on the full surface of the thoracic aorta using four-dimensional flow MRI. *Magn Reson Med*. 2015;73:1216-27.
39. Ha H, Koo HJ, Lee JG, Kim GB, Kweon J, Lee SJ *et al*. Association between flow skewness and aortic dilatation in patients with aortic stenosis. *Int J Cardiovasc Imaging*. 2017;33:1969-1978.
40. Geiger J, Markl M, Herzer L, Hirtler D, Loeffelbein F, Stiller B *et al*. Aortic flow patterns in patients with Marfan syndrome assessed by flow-sensitive four-dimensional MRI. *J Magn Reson Imaging*. 2012;35:594-600.
41. Wang HH, Chiu HH, Tseng WY and Peng HH. Does altered aortic flow in marfan syndrome relate to aortic root dilatation? *J Magn Reson Imaging*. 2016;44:500-8.
42. Hope TA, Markl M, Wigstrom L, Alley MT, Miller DC and Herfkens RJ. Comparison of flow patterns in ascending aortic aneurysms and volunteers using four-dimensional magnetic resonance velocity mapping. *J Magn Reson Imaging*. 2007;26:1471-9.
43. von Spiczak J, Crelier G, Giese D, Kozerke S, Maintz D and Bunck AC. Quantitative Analysis of Vortical Blood Flow in the Thoracic Aorta Using 4D Phase Contrast MRI. *PLoS One*. 2015;10:e0139025.
44. Weigang E, Kari FA, Beyersdorf F, Luehr M, Etz CD, Frydrychowicz A *et al*. Flow-sensitive four-dimensional magnetic resonance imaging: flow patterns in ascending aortic aneurysms. *Eur J Cardiothorac Surg*. 2008;34:11-6.
45. Barker AJ, van Ooij P, Bandi K, Garcia J, Albaghdadi M, McCarthy P *et al*. Viscous energy loss in the presence of abnormal aortic flow. *Magn Reson Med*. 2014;72:620-8.
46. Frydrychowicz A, Markl M, Hirtler D, Harloff A, Schlensak C, Geiger J *et al*. Aortic Hemodynamics in Patients With and Without Repair of Aortic Coarctation: In Vivo Analysis by 4D Flow-Sensitive Magnetic Resonance Imaging. *Invest Radiol*. 2011;46:317-325.
47. Hope MD, Meadows AK, Hope TA, Ordovas KG, Saloner D, Reddy GP *et al*. Clinical evaluation of aortic coarctation with 4D flow MR imaging. *J Magn Reson Imaging*. 2010;31:711-8.
48. LaDisa JF, Jr., Dholakia RJ, Figueroa CA, Vignon-Clementel IE, Chan FP, Samyn MM et al. Computational simulations demonstrate altered wall shear stress in aortic coarctation patients treated by resection with end-to-end anastomosis. *Congenit Heart Dis*. 2011;6:432-43.
49. LaDisa JF, Jr., Figueroa CA, Vignon-Clementel IE, Kim HJ, Xiao N, Ellwein LM *et al*. Computational simulations for aortic coarctation: representative results from a sampling of patients. *J Biomech Eng*. 2011;133:091008.
50. Andersson M, Lantz J, Ebbers T and Karlsson M. Quantitative Assessment of Turbulence and Flow Eccentricity in an Aortic Coarctation: Impact of Virtual Interventions. *Cardiovasc Eng Technol*. 2015;6:281-93.
51. Dillon-Murphy D, Noorani A, Nordsletten D and Figueroa CA. Multi-modality image-based computational analysis of haemodynamics in aortic dissection. *Biomech Model Mechanobiol*. 2016;15:857-76.
52. Karmonik C, Partovi S, Muller-Eschner M, Bismuth J, Davies MG, Shah DJ *et al*. Longitudinal computational fluid dynamics study of aneurysmal dilatation in a chronic DeBakey type III aortic dissection. *J Vasc Surg*. 2012;56:260-3 e1.

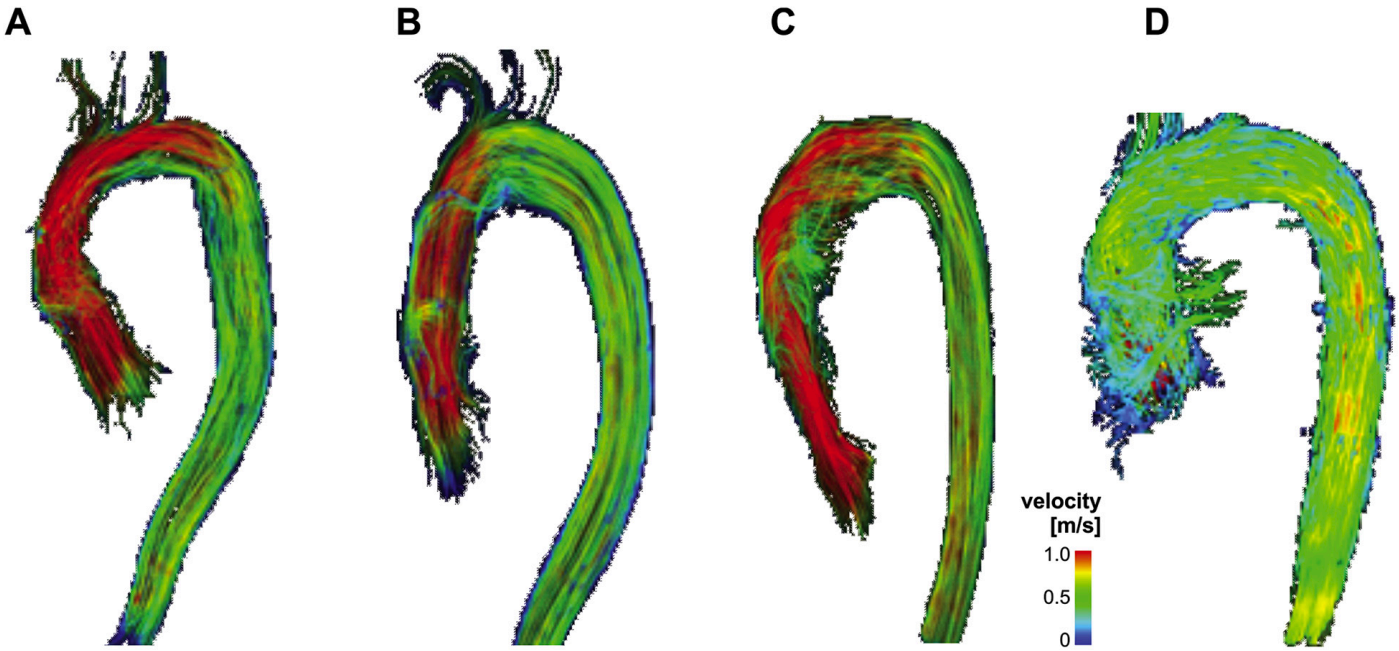
53. Strotzer M, Aebert H, Lenhart M, Nitz W, Wild T, Manke C *et al*. Morphology and hemodynamics in dissection of the descending aorta. Assessment with MR imaging. *Acta Radiol*. 2000;41:594-600.
54. Francois CJ, Markl M, Schiebler ML, Niespodzany E, Landgraf BR, Schlensak *et al*. Four-dimensional, flow-sensitive magnetic resonance imaging of blood flow patterns in thoracic aortic dissections. *J Thorac Cardiovasc Surg*. 2013;145:1359-66.
55. Karmonik C, Bismuth J, Davies MG, Shah DJ, Younes HK and Lumsden AB. A computational fluid dynamics study pre- and post-stent graft placement in an acute type B aortic dissection. *Vasc Endovascular Surg*. 2011;45:157-64.
56. Tan FPP, Xu XY, Torii R, Wood NB, Delahunty N, Mullen M *et al*. Comparison of Aortic Flow Patterns Before and After Transcatheter Aortic Valve Implantation. *Cardiovascular Engineering and Technology*. 2012;3:123-135.
57. Trauzeddel RF, Lobe U, Barker AJ, Gelsinger C, Butter C, Markl M *et al*. Blood flow characteristics in the ascending aorta after TAVI compared to surgical aortic valve replacement. *Int J Cardiovasc Imaging*. 2016;32:461-7.
58. Kozerke S, Hasenkam JM, Pedersen EM and Boesiger P. Visualization of flow patterns distal to aortic valve prostheses in humans using a fast approach for cine 3D velocity mapping. *J Magn Reson Imaging*. 2001;13:690-8.
59. Leuprecht A, Kozerke S, Boesiger P and Perktold K. Blood flow in the human ascending aorta: a combined MRI and CFD study. *Journal of Engineering Mathematics*. 2003;47:387-404.
60. Hellmeier F, Nordmeyer S, Yevtushenko P, Bruening J, Berger F, Kuehne T *et al*. Hemodynamic Evaluation of a Biological and Mechanical Aortic Valve Prosthesis Using Patient-Specific MRI-Based CFD. *Artif Organs*. 2018;42:49-57.
61. Keller EJ, Malaisrie SC, Kruse J, McCarthy PM, Carr JC, Markl M *et al*. Reduction of aberrant aortic haemodynamics following aortic root replacement with a mechanical valved conduit. *Interact Cardiovasc Thorac Surg*. 2016;23:416-23.
62. van Kesteren F, Wollersheim LW, Baan J, Jr., Nederveen AJ, Kaya A, Boekholdt SM *et al*. Four-dimensional flow MRI of stented versus stentless aortic valve bioprostheses. *Eur Radiol*. 2018;28:257-264.
63. Cheng Z, Kidher E, Jarral OA, O'Regan DP, Wood NB, Athanasiou T *et al*. Assessment of Hemodynamic Conditions in the Aorta Following Root Replacement with Composite Valve-Conduit Graft. *Ann Biomed Eng*. 2015.
64. Midulla M, Moreno R, Baali A, Chau M, Negre-Salvayre A, Nicoud F *et al*. Haemodynamic imaging of thoracic stent-grafts by computational fluid dynamics (CFD): presentation of a patient-specific method combining magnetic resonance imaging and numerical simulations. *Eur Radiol*. 2012;22:2094-102.
65. Oechtering TH, Hons CF, Sieren M, Hunold P, Hennemuth A, Huellebrand M *et al*. Time-resolved 3-dimensional magnetic resonance phase contrast imaging (4D Flow MRI) analysis of hemodynamics in valve-sparing aortic root repair with an anatomically shaped sinus prosthesis. *J Thorac Cardiovasc Surg*. 2016;152:418-427 e1.
66. Semaan E, Markl M, Malaisrie SC, Barker A, Allen B, McCarthy P *et al*. Haemodynamic outcome at four-dimensional flow magnetic resonance imaging following valve-sparing aortic root replacement with tricuspid and bicuspid valve morphology. *Eur J Cardiothorac Surg*. 2014;45:818-25.
67. Bogren HG, Buonocore MH and Follette DM. Four-dimensional aortic blood flow patterns in thoracic aortic grafts. *J Cardiovasc Magn Reson*. 2000;2:201-8.
68. Collins JD, Semaan E, Barker A, McCarthy PM, Carr JC, Markl M *et al*. Comparison of Hemodynamics After Aortic Root Replacement Using Valve-Sparing or Bioprosthetic Valved Conduit. *Ann Thorac Surg*. 2015;100:1556-62.

606 69. Torii R, El-Hamamsy I, Donya M, Babu-Narayan SV, Ibrahim M, Kilner PJ *et al*. Integrated
607 morphologic and functional assessment of the aortic root after different tissue valve root replacement
608 procedures. *J Thorac Cardiovasc Surg*. 2012;143:1422-8.
609 70. Frydrychowicz A, Berger A, Stalder AF and Markl M. Preliminary results by flow-sensitive
610 magnetic resonance imaging after Tiron David I procedure with an anatomically shaped ascending
611 aortic graft. *Interact Cardiovasc Thorac Surg*. 2009;9:155-8.
612 71. Markl M, Draney MT, Miller DC, Levin JM, Williamson EE, Pelc NJ *et al*. Time-resolved
613 three-dimensional magnetic resonance velocity mapping of aortic flow in healthy volunteers and
614 patients after valve-sparing aortic root replacement. *J Thorac Cardiovasc Surg*. 2005;130:456-63.
615 72. Kvitting JP, Ebbers T, Wigstrom L, Engvall J, Olin CL and Bolger AF. Flow patterns in the
616 aortic root and the aorta studied with time-resolved, 3-dimensional, phase-contrast magnetic
617 resonance imaging: implications for aortic valve-sparing surgery. *J Thorac Cardiovasc Surg*.
618 2004;127:1602-7.
619 73. Bollache E, Fedak PWM, van Ooij P, Rahman O, Malaisrie SC, McCarthy PM *et al*.
620 Perioperative evaluation of regional aortic wall shear stress patterns in patients undergoing aortic
621 valve and/or proximal thoracic aortic replacement. *J Thorac Cardiovasc Surg*. 2017.
622 74. Singh SD, Xu XY, Pepper JR, Treasure T and Mohiaddin RH. Biomechanical properties of
623 the Marfan's aortic root and ascending aorta before and after personalised external aortic root support
624 surgery. *Med Eng Phys*. 2015;37:759-66.
625 75. Singh SD, Xu XY, Pepper JR, Izgi C, Treasure T and Mohiaddin RH. Effects of aortic root
626 motion on wall stress in the Marfan aorta before and after personalised aortic root support (PEARS)
627 surgery. *J Biomech*. 2016;49:2076-84.
628 76. Singh SD, Xu XY, Wood NB, Pepper JR, Izgi C, Treasure T *et al*. Aortic flow patterns
629 before and after personalised external aortic root support implantation in Marfan patients. *J Biomech*.
630 2016;49:100-11.
631 77. Bissell MM, Dall'Armellina E and Choudhury RP. Flow vortices in the aortic root: in vivo
632 4D-MRI confirms predictions of Leonardo da Vinci. *Eur Heart J*. 2014;35:1344.
633


A
B
C


A
B
C
D


A healthy volunteer
B aorta size control
C RL-BAV
D RN-BAV
left-anterior view
velocity [m/s]
1.0
0.5
0
arch
AAo
LVOT
DAo
AV
flow jet
anterior view
velocity [m/s]
1.0
0.5
0
arch
AAo
LVOT
DAo


A
B
C
D
velocity
[m/s]
1.0
0.5
0

Overview of PC-CMR

Velocity encoding

MRI can be made flow-sensitive by applying a bipolar gradient between excitation and readout. The effect on the phase of stationary spins is exactly cancelled out by the successive gradients. However, moving spins accumulate a phase difference proportional to the component of velocity in the direction of the phase-encoding gradient (**Figure S1)**. A velocity encoding (VENC) value is pre-specified such that spins travelling at that velocity will experience a phase change of 180˚. If the velocity of spins exceeds this value, then aliasing will occur leading to underestimation of peak velocity. Imaging of flowing blood is performed with prospective or retrospective ECG gating such that time-resolved data is acquired throughout the cardiac cycle.

Velocity-encoding is typically performed in one direction on a 2D image – and may be acquired in any chosen direction relative to the imaging plane (**Figure S2)**. Alternatively, 4D flow CMR is an emerging technology which acquires a volume of images with flow velocities encoded in each orthogonal axis. These techniques have demonstrated low observer variability, test-retest reliability, and good correlation between 2D and 4D approaches[1]. They potentially offer some benefits over velocity assessment with Doppler ultrasound, which is operator dependent and only allows determination of blood flow velocity in the direction of the ultrasound beam. Contrast is not required these scans but may be given if a more comprehensive cardiac assessment is being performed.

2D PC-CMR

2D PC-CMR is routinely employed as a diagnostic and research tool for flow volume quantification[2]. It involves encoding time-resolved velocity (normally in 1, but up to 3 directions), perpendicular to a 2D transverse plane (i.e. through-plane flow) at a selected

location in the aorta, shown in **Figure S3** just above the AV and at the pulmonary bifurcation in the descending thoracic aorta (DTA). During 2D PC-CMR assessment, an anatomic scan of the aorta is first obtained to delineate the area of interest, followed by acquisition of ECG-gated phase-contrast (PC) imaging during several breath holds (done to minimise breathing artefact). These take between 8-15 seconds each (depending on heart rate, spatial/temporal resolution and number of flow encoding detections). PC imaging can be easily reconstructed to produce colour images (**Figure S4)** and time-velocity/flow curves, and used to calculate standardised parameters, including peak velocity, stroke volume, net flow, regurgitant fraction, and shunt flows[1]. More complex variables such as wall-shear stress (WSS) can be estimated directly but limited by velocity that has been encoded in just a single direction. By combining the velocity images with computational fluid dynamics (CFD) techniques (elaborated on below), more complex variables can be calculated to a high spatial and temporal resolution.

4D flow CMR

4D flow CMR (also called 4D PC-MRI and time-resolved 3D velocity mapping) involves encoding time-resolved velocity (in all 3 directions) within an entire vessel or structure of interest. Whilst available since the 90's, it is mainly used for research purposes. Practically, it differs from 2D PC-CMR by selecting a whole volume of interest (e.g. the entire thoracic aorta), rather than placement of a single plane, with prospective or retrospective ECG gating and navigator gating of the diaphragm motion applied during velocity encoding to reduce breathing artefact. Scan times are understandably longer than 2D scanning (5-15 minutes using protocols and imaging parameters that are starting to become standardised[2]), but without the need for breath holds by using image registration.

4D flow CMR allow similar variables to be calculated as listed above with 2D PC-CMR, with comparable accuracy[2]. In addition, there are three key benefits to 4D flow imaging. Firstly, it

allows direct visualisation of 3D cardiovascular haemodynamics and flow patterns. Time-resolved pathlines represent traces and speed of blood flow throughout the cardiac cycle (**Figure S3)**[1]. Streamlines represent traces along the instantaneous 3D velocity field. Secondly, it is possible to retrospectively quantify blood flow at any point within the volumetric coverage of the scan. 2D scans are limited to the information collected in planes selected at the time of the scan. Thirdly, the technique allows direct estimation of additional variables including 3D pressure maps and energy loss[3].

Many of the variables derived from 4D flow imaging cannot be ascertained non-invasively from other diagnostic modalities. However, it should be noted that several variables are estimations, with accuracy dependent on acquisition parameters and multiple mathematical assumptions. The accuracy and reliability of WSS (which is estimated by near-wall velocity gradients) has been questioned given the challenges in vessel wall segmentation[4]. Due to the low spatial resolution of MRI, blood flow velocities cannot be measured any closer to the aortic wall than 1000-1200 μm (affecting the calculation of velocity gradients), which is why the technique underestimates WSS[5]. The temporal resolution of MRI also limits the ability to study the true dynamic and subtle nature of WSS patterns in animal vessels. Estimating WSS is complicated further by the exact method used to reproduce the velocity profile on which the gradient is calculated. Methods include linear extrapolation between the velocity in two voxels, assumption of parabolic velocity distributions, Lagrangian interpolation polynomials, and B-spline interpolation[5]. As with 2D PC-CMR, improvement on the accuracy and depth of variables calculated can be achieved with the assistance of CFD techniques discussed below. **Table A** summarises the differences between 2D PC-CMR and 4D flow CMR.

Typical work flow in analysing 4D flow CMR data

Several steps are required to analyse 4D flow CMR data. Until recently, there was no standardised method to deal with for the technical challenges in 4D flow CMR data analysis, such as artefact, parameter setting, post-processing, and data analysis[1]. A recent consensus statement was released with view to standardising 4D flow acquisitions[2], with steps illustrated in **Figure S5**. This has the added advantage of making studies from different institutions comparable and allow us to develop normalised population values for haemodynamic variables.

Furthermore, relative novices are now able to perform the final stage of data analysis due to the emergence of powerful desktop software which automate much of the process. **Figure S6** demonstrates the use of such software (PIE Medical) in calculating time averaged WSS from a healthy volunteer (which took less than ten minutes). A few groups have started using custom built programs to analyse very large 4D flow datasets (e.g. extraction of certain parameters from multiple patients scans from an institutions MRI database).

Various cloud-based services also now exist, which allow storage and analysis of CMR data (e.g. Arterys). Such services offer the theoretical advantage of flexible storage services and use of specialised technical analysis tools (which would usually require costly infrastructure) on a pay as you go basis to institutions of all sizes. However, a number of challenges relating to regulation, privacy, and data security will need to be addressed prior to widespread adoption[6].

Other MRI techniques which may supplement flow data

The above techniques do not give detailed information on the circumferential/axial aortic wall stresses and strains which arise due to pulsatile blood flow. A modified PC-CMR protocol called Displacement Encoding using Stimulated Echoes (DENSE) has been developed to

record tissue displacement[7] while strain encoding (SENC) MRI techniques can encode tissue strain in acquired images (through-plane strain data). Although initially developed for the assessment of myocardial contractility, newer studies are using DENSE to assess aortic distensibility, by using steady-state free precession MRI imaging with ECG gating. Cross-sectional area (after segmentation) is measured from which distensibility can be calculated and mapped regionally[8]. There are currently no accurate ways of using MRI to assess the stress within an aortic plaque, or within an area of aorta at risk (e.g. aneurysmal segment). Most advancements in this area have been made with CFD techniques which will be elaborated on below.

Computational fluid dynamics modelling of the thoracic aorta

CFD modelling techniques are a branch of fluid mechanics. They involve solving complex differential equations (Navier-Stokes equation, NSEs) to simulate fluid flow and have been used extensively in solving problems in the fields of aeronautics and chemical engineering. Over the last two decades, these techniques have been applied to healthcare in simulating blood and other flows (e.g. cerebrospinal and lymphatic fluid) around the body. A number of groups have used CFD in combination with PC-CMR to produce more sophisticated analysis of thoracic aortic biomechanics. Whilst a detailed description of CFD is beyond the scope of this article, an overview of the steps required is given below. CFD is computationally expensive and time consuming, but offers the benefit of being able to provide more advanced hemodynamic variables (at a high temporal and spatial resolution) than PC-CMR alone.

The workflow to solve the NSEs involves several steps including pre-processing, assigning material properties for blood, setting boundary conditions, post-processing, verification and validation. Most CFD simulations are performed using both commercially available (e.g. ANSYS or FlowVision), and in-house software packages (e.g. custom-made programs within

CRIMSON or SimVascular). Prior to simulating blood flow, the geometrical boundaries of the aorta being assessed need to be created. There are two approaches to setting geometrical boundaries: idealised and patient-specific. Idealised geometries are essentially simplified copies of a vessel, e.g. a cylindrical straight or "candy cane" tube that is designed to represent the DTA. The superior approach is the creation of 3D patient-specific geometries, in which MRI or computed tomography (CT) images are used to accurately create the boundaries which take into account all the complexities of a real vessel[9]. This model is then discretized into a finite number of small elements or cells. It is within these cells that the complex differential equations (NSE) are solved. The greater the number of individual cells, the greater the accuracy of the simulation, but the more time consuming the analysis. These cells can be contained in either structured (hexahedral) or unstructured (tetrahedral) meshes. **Figure S7** demonstrates the creation of a 3D geometry from an MRI scan of a patient following root replacement, and the subsequent creation of a structured mesh.

To simulate flow, material properties of the blood within the created geometry need to be defined. Blood is a complex fluid with properties dependent on a range of physical and environmental parameters. Although it exhibits non-Newtonian behaviour, it is usually treated as a Newtonian fluid in CFD analyses of arterial flow. This is based on the fact that experimental studies show that at high shear rates in large and medium arteries, the viscosity of human blood is relatively constant[10]. In addition to the material properties, the appropriate flow model needs to be selected. Commonly, a laminar flow assumption is used. However, *in-vivo* measurements confirm that there is transition to turbulence at the level of the aortic valve, in the ascending aorta, and in the presence of coarctation and dissection. In order to capture this, transitional flow models (such as shear stress transport model) or large-eddy simulation have been used to model aortic flow[11, 12].

Simulation within the chosen geometry requires the input of physiological boundary conditions at the inlet (the start of the model), and at the outlet (at the end of the model). It is based on these parameters the subsequent NSEs are solved to determine blood flow patterns.

At the inlet, boundary conditions can be idealised (e.g. flat or a parabolic profile) or patient-specific from actual imaging (e.g. from PC-CMR), which should be time-varying. Outlet conditions in most CFD simulations are either a fixed flow rate or pressure, or time-varying pressures/velocities. Boundary conditions play an important role in CFD simulations and should be carefully chosen, as it has been shown that they can drastically impact the obtained results. Literature studies suggest that 3D patient-specific time-varying velocity profiles and 3-element Windkessel models should be used for open-loop aortic models, as inlet and outlet boundary conditions respectively. These boundary conditions showed the best agreement with *in-vivo* velocity and pressure data. The aortic wall is typically assumed to be rigid in most CFD studies. Few studies take in to account organs and tissues surrounding the aortic wall. Several ligaments and structures (e.g. the spine, pericardium, ligamentum arteriosum) impact the resultant displacement and deformation the aorta experiences because of pulsatile flow. Some authors have introduced arterial wall boundary conditions which attempt to approximate reality.

Following the configuration of above boundary conditions, the governing NSEs are solved and the simulation results can be assessed. Depending on the size and complexity of the computational domain, this analysis can take from hours to many days. Various haemodynamic parameters are calculable, including WSS, turbulent kinetic energy, compliance, relative residence time, and visualisation of streamlines and particle tracking[13]. These are calculable at multiple levels and can often be plotted as 3D models. The interpretation of this vast amount

of data is challenging and requires experience and judgement as to what is of clinical significance. Following the calculation of variables, verification is performed. This is an assessment of the accuracy of the numerical solution for the mathematical model. Validation involves determining to what degree the model is an accurate representation of reality. This can be done by comparing the results of modelling and real experimental data. **Figure S8** demonstrates an example of the use of CFD in visualisation of calculated flow streamlines in a patient before and after composite aortic root replacement with a mechanical (valve) conduit.

References

1. Markl M, Kilner PJ and Ebbers T. Comprehensive 4D velocity mapping of the heart and great vessels by cardiovascular magnetic resonance. *J Cardiovasc Magn Reson*. 2011;13:7.
2. Dyverfeldt P, Bissell M, Barker AJ, Bolger AF, Carlhall CJ, Ebbers T, Francios CJ, Frydrychowicz A, Geiger J, Giese D, Hope MD, Kilner PJ, Kozerke S, Myerson S, Neubauer S, Wieben O and Markl M. 4D flow cardiovascular magnetic resonance consensus statement. *J Cardiovasc Magn Reson*. 2015;17:72.
3. Binter C, Gotschy A, Sundermann SH, Frank M, Tanner FC, Luscher TF, Manka R and Kozerke S. Turbulent Kinetic Energy Assessed by Multipoint 4-Dimensional Flow Magnetic Resonance Imaging Provides Additional Information Relative to Echocardiography for the Determination of Aortic Stenosis Severity. *Circ Cardiovasc Imaging*. 2017;10.
4. Burris NS and Hope MD. 4D flow MRI applications for aortic disease. *Magn Reson Imaging Clin N Am*. 2015;23:15-23.
5. Pantos I, Patatoukas G, Efstathopoulos EP and Katritsis D. In vivo wall shear stress measurements using phase-contrast MRI. *Expert Rev Cardiovasc Ther*. 2007;5:927-38.
6. Kawel-Boehm N and Bluemke DA. Cardiovascular imaging environment: will the future be cloud-based? *Expert Review of Medical Devices*. 2017;14:521-528.
7. Lin AP, Bennett E, Wisk LE, Gharib M, Fraser SE and Wen H. Circumferential strain in the wall of the common carotid artery: comparing displacement-encoded and cine MRI in volunteers. *Magn Reson Med*. 2008;60:8-13.
8. Cavalcante JL, Lima JA, Redheuil A and Al-Mallah MH. Aortic stiffness: current understanding and future directions. *J Am Coll Cardiol*. 2011;57:1511-22.
9. Mori D and Yamaguchi T. Computational fluid dynamics modeling and analysis of the effect of 3-D distortion of the human aortic arch. *Comput Methods Biomech Biomed Engin*. 2002;5:249-60.
10. Pedley TJ. *The fluid mechanics of large blood vessels*. Cambridge: Cambridge University Press; 1980.
11. Vergara C, Le Van D, Quadrio M, Formaggia L and Domanin M. Large eddy simulations of blood dynamics in abdominal aortic aneurysms. *Med Eng Phys*. 2017;47:38-46.
12. Cheng Z, Tan FP, Riga CV, Bicknell CD, Hamady MS, Gibbs RG, Wood NB and Xu XY. Analysis of flow patterns in a patient-specific aortic dissection model. *J Biomech Eng*. 2010;132:051007.
13. Caballero ADL, S. A Review on Computational Fluid Dynamics Modelling in Human Thoracic Aorta. *Cardiovascular Engineering and Technology,*. 2013;4:103-130.
14. Markl M, Schnell S and Barker AJ. 4D flow imaging: current status to future clinical applications. *Curr Cardiol Rep*. 2014;16:481.

Tables

Table A: 2D PC-CMR vs. 4D flow CMR

	2D PC-CMR	4D flow CMR
Current use	Widespread clinical use	Mainly research
Velocity encoding	Usually in one direction, in a pre-defined plane	Three directional, over an entire volume of vessel
Respiratory control	Breath holds	Free breathing
Scan time	5-20 mins	5-15 seconds per 2D plane
Data analysis	Standardised with clearly defined variables (peak velocity, stroke volume, flow, regurgitant fraction, shunts)	Non-standardised, multiple options for analysis
Flow visualisation	2D velocity profiles	3D time resolved pathlines and streamlines
Flow quantification	Can be performed only at pre-defined 2D planes	Can be retrospectively performed anywhere within volumetric coverage
Other calculable variables	Wall shear stress, pulse-wave velocity	Wall shear stress, pulse-wave velocity, 3D pressure difference maps, turbulent kinetic energy, energy loss, pulse-wave velocity, flow displacement, flow jet angle

Adapted from Markl et al.[14]

Figures

Figure S1: Diagram illustrating phase differences generated due to moving spins of particles (redrawn with reference from mriquestions.com)

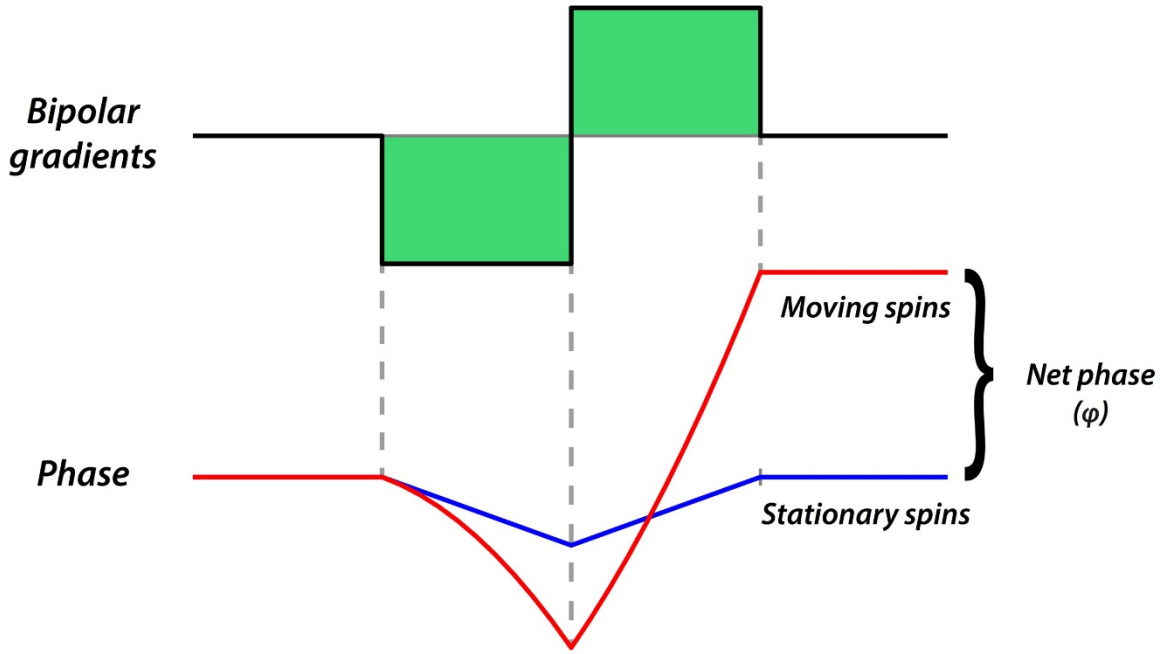


Figure S2: VENC images where stationary tissue is grey, and moving tissue or blood is either white or black (depending on direction). The greater the intensity of the white or blackness indicates greater velocity.

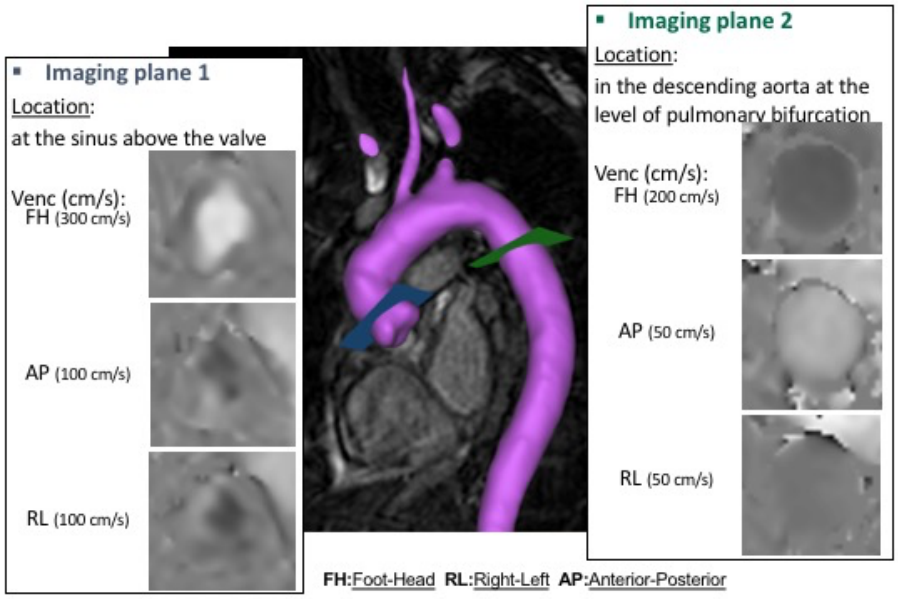


Figure S3: Time-resolved streamlines representing traces and speed of blood flow throughout the cardiac cycle

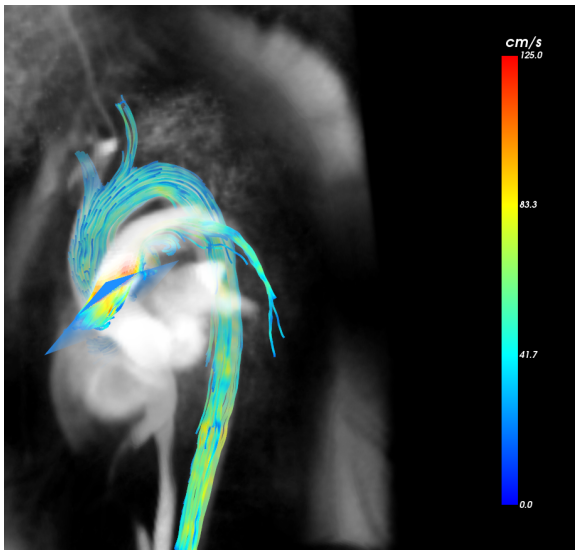


Figure S4: Software reconstruction of VENC images

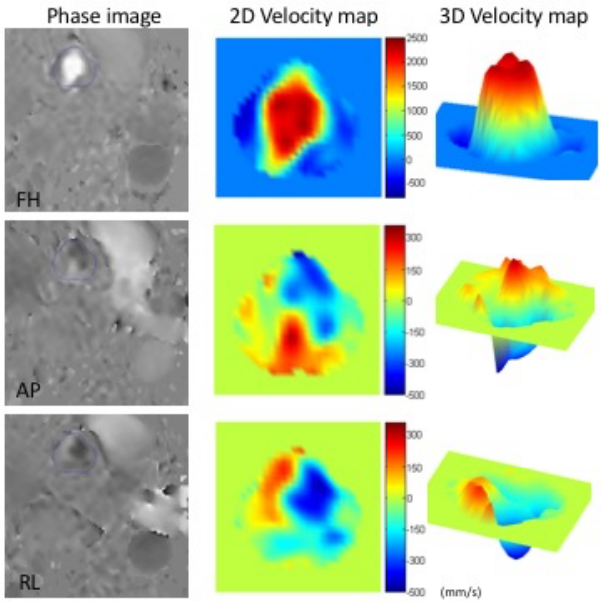


Figure S5: Proposed workflow steps in 4D flow MR data acquisition (from Dyverfeldt et al.[2], reproduced with permission of copyright holder Dr. Petter Dyverfeldt)

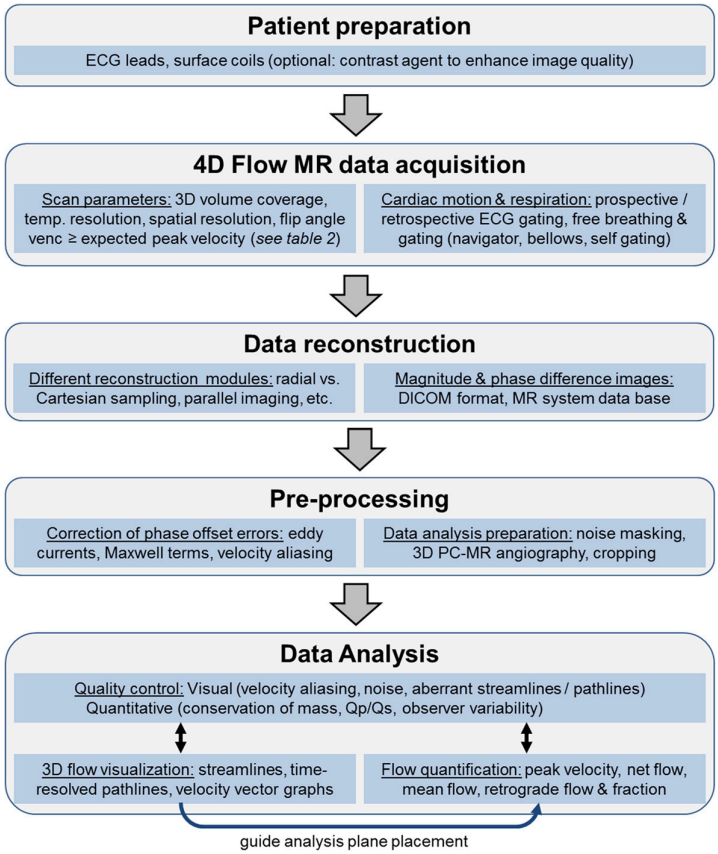


Figure S6: WSS calculation directly from 4D flow MRI using PIE medical software

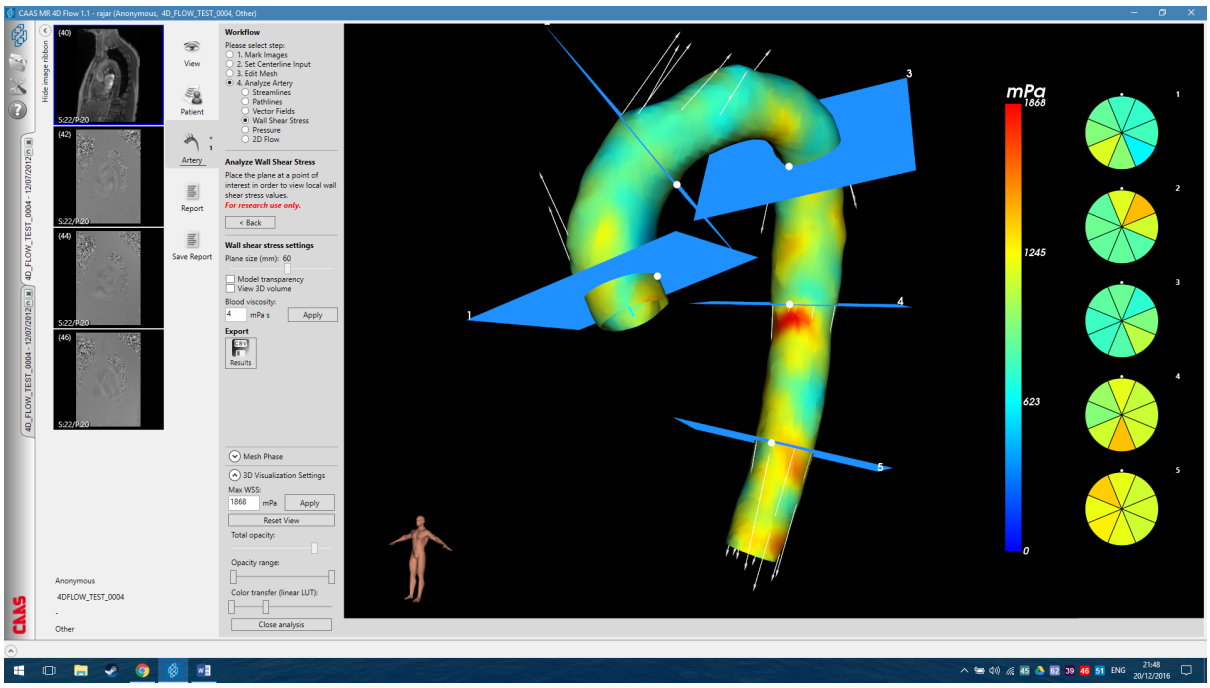


Figure S7: Creation of a 3D geometry from an MRI scan of a patient following root replacement, and the subsequent creation of a structured mesh

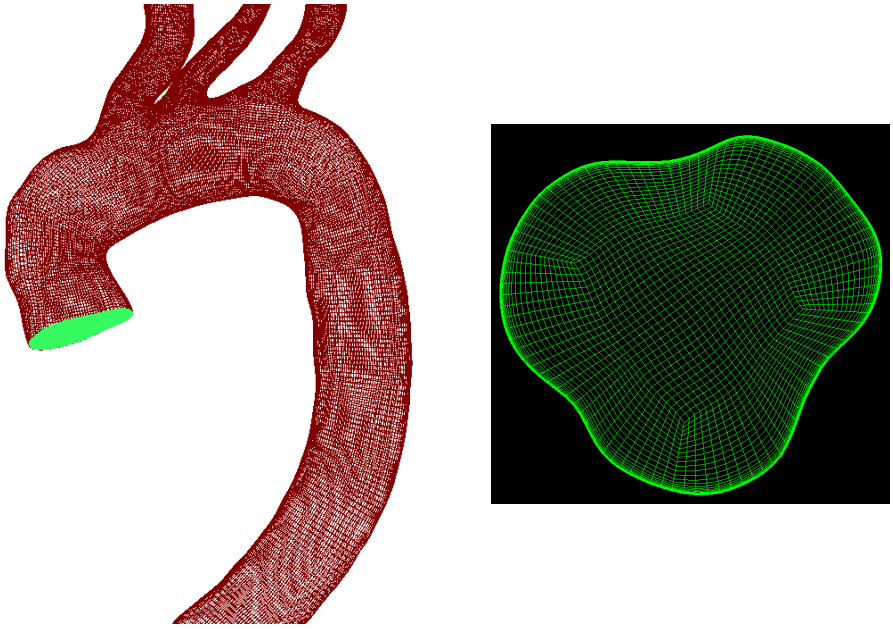


Figure S8: Calculated flow streamlines in a patient before and after composite aortic root replacement with a mechanical conduit.

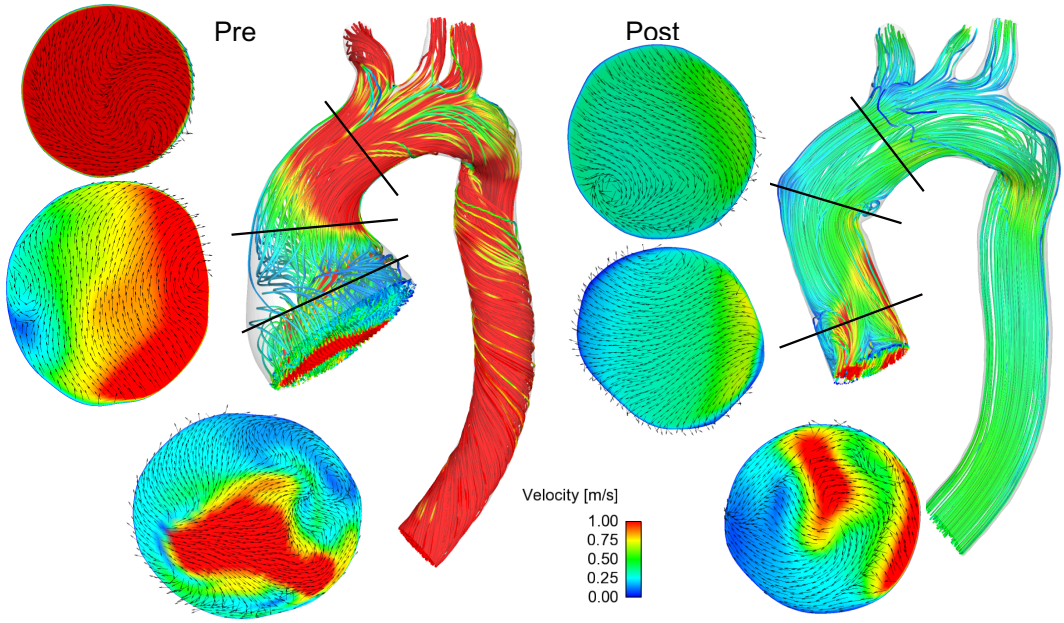


TABLE S1 – Healthy individuals

Author & Year	Number of patients	Technique used, variables calculated, software used	Key findings / useful images
Bogren et al. 2004[8]	41	4D flow CMR Particle paths and streamlines, vortex formation MRI View (custom)	Flow patterns compared in healthy patients (age matched) with patients with coronary artery disease (aortic sizes unmatched). In elderly patients, systolic velocities and time taken for particles to travel to descending aorta longer. This time was longer in those with coronary artery disease. Retrograde velocity was higher in coronary artery disease patients and the elderly. Chaotic and irregular flow seen in most coronary artery disease patients. Most pronounced changes seen in young coronary artery disease patients. In most patients and controls, right handed helical flow observed in the ascending aorta, and left handed helical flow in the descending aorta.
Stalder et al. 2011[10]	30	4D flow CMR Flow, Womersley, Strouhal, Reynolds, and critical Reynolds numbers (measures of flow instability) MATLAB (in-house), The Mathworks, USA	Multiple measures of flow instability assessed in a cohort of young healthy volunteers. The average Reynolds number was higher in the ascending aorta (4500), than in the arch (3400) descending aorta (4200). Flow instabilities (based on critical Reynolds numbers) were seen in over half of healthy patients in the ascending and descending aorta, but uncommonly seen in the arch. Instabilities (supracritical Reynolds number) were significantly more common in men, and correlated with body weight, aortic diameter and cardiac output.

Frydrychowicz et al. 2008[6]	12	4D flow CMR WSS, OSI helical and vortical flow MATLAB (in-house), The Mathworks, USA EnSight, CEI, USA	Flow pattern assessment in cohort of healthy volunteers and one patient before and after aortic intervention. In normal patients, characteristic right-handed helical flow observed in the ascending aorta, with vortex seen in only one. Region of low WSS and high OSI consistently seen at the inner curvature of the ascending aorta In the single patient with aortic stenosis, substantial flow changes around the stenosis. Little evidence of oscillatory or retrograde flow seen in healthy individuals. Little inter-individual differences in WSS and OSI between healthy individuals.
Frydrychowicz et al. 2009[7]	31	4D flow CMR WSS, OSI MATLAB (in-house), The Mathworks, USA EnSight, CEI, USA	Segmental WSS and OSI assessed in a cohort of young healthy patients. Marked regional differences both within each plane, and when comparing different planes in WSS and OSI. The atherogenic pattern of low WSS and high OSI closely matched locations of typical atherosclerotic lesions at the inner aortic curvature and supraaortic branches. Authors created reference maps for averaged values of WSS for entire cohort. This showed: in the proximal aorta low WSS and high OSI occurred along left inner curve. In the arch, low WSS and high OSI moved toward the out curve. In the proximal descending aorta, the inner curve was exposed to low WSS and high OSI, and more distally values were distributed more homogeneously.
Stalder et al. 2011[10]	62	4D flow CMR Helix and vortex formation, 3D particle traces and streamlines	Analysis of 62 healthy volunteers to examine impact of age and arch geometry on helix and vortex formation. Aortic diameter and age correlated with the number of detected vortices. Helical flow was the typical pattern in standard crook-shaped arches (right-handed). With altered shapes, and increasing age, helicity was less common. In summary, aortic geometry showed less of an impact on secondary blood flow patterns than age and aortic diameter.

		EnSight, CEI, USA	
Garcia et al. 2018[12]	98	4D flow CMR Peak flow velocity, velocity distribution MATLAB (in-house), The Mathworks, USA	Analysis of 98 healthy volunteers to examine impact of age and gender on aortic blood flow peak velocity and velocity distribution. Peak velocity was significantly different between age groups, with greater skewness and kurtosis in >40-year olds when compared to <21-year olds. Significant differences were seen between men and women for all velocity descriptors.
Morbiducci et al. 2010[11]	5	4D flow CMR Helix formation (helical flow index and local normalised helicity), particle traces Analyze, Mayo Clinic, USA MATLAB (in-house), The Mathworks, USA	Assessment of helical flow in a group of healthy volunteers. Two key findings: helical content varies during systole (highest after the systolic peak), and helical flow is common in normal individuals. The pattern seen was: following peak net forward flow and up to the end of systole, coherent helical structures appear (located at the inner wall), in the deceleration phase high more coherent helicity (associated with helical and bi-helical structures) are seen in the ascending aorta and upper arch.

TABLE S2 – Aortic valve disease

Author & Year	Number of patients	Technique used, variables calculated, software used	Key findings / useful images
Allen et al. 2015[34]	40	4D flow CMR Helical flow, pressure gradient MATLAB (in-house), The Mathworks, USA EnSight, CEI, USA	Assessment of flow patterns in those with hypertrophic cardiomyopathy (basal-septal phenotype) compared with controls. Patients had greater helical flow (worse in obstructive vs. non-obstructive) in the proximal aorta. Helical flow correlated with outflow tract gradient and systolic anterior motion of the mitral valve.
Allen et al. 2016[13]	75	4D flow CMR WSS, peak elocity MATLAB (in-house), The Mathworks, USA Mimics, Materialise, Belgium	Comparison of flow patterns in those with bicuspid aortic valve being treated with and without beta-blocker, with a further control group. Both bicuspid groups had higher peak and mean WSS compared to control group. WSS and peak velocity were not lower in the beta blocker group. Aortic stenosis severity and aortic diameter was associated with significantly increased mean WSS.
Barker et al. 2010[22]	30	2D PC- CMR WSS, flow rates, regurgitant fraction, shear range indices	Comparison of haemodynamic parameters in cohort of bicuspid valve and control patients. The bicuspid group had significantly different circumferentially averaged and positional WSS at systole. WSS and shear range indices correlated with aortic size.

		MATLAB (in-house), The Mathworks, USA ARGUS, Siemens, Germany	
Barker et al. 2012[28]	60	4D flow CMR WSS MATLAB (in-house), The Mathworks, USA EnSight, CEI, USA	Comparison of flow patterns in bicuspid valved patients and matched controls. WSS patterns in the right-left valved patients were significantly higher in the ascending aorta, independent of degree of stenosis. Right-left fusion led to a distinct jet flow pattern, with impingement on the right anterior ascending aorta.
Bissell et al. 2013[14]	142	4D flow CMR WSS, systolic flow angle, helical flow MATLAB (in-house), The Mathworks, USA EnSight, CEI, USA	Comparison of flow patterns in bicuspid patients and healthy volunteers. The bicuspid group (which had larger aortas) had predominantly abnormal right-handed helical flow, higher helical flow, greater systolic flow angle, and greater systolic WSS. Those with Right-Non bicuspid fusion showed more severe flow abnormalities than Right-left patients. Degree of aortic stenosis also worsened WSS. Younger bicuspid patients had normal sized aortas and normally functioning valves, but showed abnormal flow patterns including increased flow angle, helical flow and a greater tendency towards left handed helical flow (in the RN group). Distensibility, strain and stiffness similar across all groups.
Burris and Hope 2015[29]	59	2D PC- CMR	Comparison of different fusion patterns of bicuspid valve, examining subsequent flow patterns. Flow displacement in Right-Left group strongly rightward, and leftward in the Right-Non

		Eccentricity, flow displacement, pattern of aortopathy Medis, Netherlands	group. Right-left group more likely to demonstrate type 2 aortopathy, and right-non type 3 aortopathy.
Della Corte et al.[23]	46	2D PC- CMR and CFD Wall strain, diameters, cusp opening angle, aortic growth rate FLUENT, Ansys Inc, USA	MRI and CFD performed in a group of normally functioning bicuspid valved patients, and healthy controls. Bicuspid valved patients had restriction of valve opening and increased systolic flow deflection, aswell as circumferential heterogenous wall strain patterns. Conjoint cusp opening angle predicted aortic growth at follow up. Computational models confirmed that restricted cusp motion can account for flow deflection on its own.
Entezari et al. 2014[24]	28	4D flow CMR Valve flow angle EnSight, CEI, USA	Comparison of haemodynamics in uni, and bicuspid valved patients compared to controls. All Right-left vales had flow jets directed towards the right anterior aorta, while Right-non fusion and unicuspid valves resulted in flow patterns towards the right posterior or posterior wall. Flow angle abnormal in patients vs. controls.
Faggiano et al. 2013[15]	8	2D PC- CMR and CFD Flow asymmetry index, systolic WSS, positive helix fraction, retrograde flow,	Use of both MRI and CFD to assess flow patterns in bicuspid and tricuspid patients with normally functioning valves. Bicuspid group had greater abnormal flow patterns including greater flow asymmetry and flow reversal, strongly localised and higher WSS, and helix formation.

		Vmtk Toolkit LifeV	
Garcia et al. 2016[78]	165	4D flow CMR Peak velocities, systolic flow displacement MATLAB (in-house), The Mathworks, USA Mimics, Materialise, Belgium	Comparison of haemodynamics between bicuspid valved patients, tricuspid valved patients with a dilated aorta, and controls. Bicuspid valved patients showed abnormal haemodynamics when compared with size matched controls. Aortic diameter was associated with peak velocity and flow displacement.
Garcia et al. 2017[32]	115	4D flow CMR Peak velocities, helical flow MATLAB (in-house), The Mathworks, USA Mimics, Materialise, Belgium	Comparison of haemodynamics between bicuspid valved patients with aortic dilatation and controls. Absolute localised normalised helicity was correlated to degree of aortic dilatation at peak systole, systolic deceleration, and middiastole, and was significantly increased with severity of aortic stenosis.
Guzzardi et al. 2015[30]	30	4D flow CMR WSS	Assessment of the relationship between WSS and regional aortic tissue remodelling in bicuspid valved patients by assessing medial elastin degeneration, and protein expression at points of maximal WSS and normal WSS. Regions of increased WSS corresponded with extracellular matrix dysregulation and elastic fiber degeneration in the ascending aorta.

		MATLAB (in-house), The Mathworks, USA EnSight, CEI, USA	
Hope et al. 2010[16]	53	4D flow CMR Helical flow EnSight, CEI, USA	Comparison of flow patterns in bicuspid and tricuspid patients, compared to controls. Nested helical flow (greater than 180 degree curvature) seen in most bicuspid patients (in those with and without aneurysm/valve stenosis) at peak systole in ascending aorta, but in none of the tricuspid or control groups. Right-left fusion gave rise to right-handed helical flow (right-anterior flow jet), whereas right-non fusion gave rise to left-handed helical flow (left-posterior flow jet).
Hope et al. 2011[17]	46	4D flow CMR Helical flow, WSS, flow eccentricity EnSight, CEI, USA Uni Freigberg flow tool, Germany	Comparison of flow patterns in bicuspid and tricuspid patients, compared to controls. Patients with bicuspid valve and eccentric systolic blood flow was found to have significantly and asymmetrically elevated WSS (independent of presence of aneurysm). Even those with bicuspid valve and normal flow had elevated WSS in the right-anterior region compared to those with tricuspid vales.
Hope et al. 2012[33]	25	4D flow CMR Flow eccentricity, longitudinal aortic growth EnSight, CEI, USA	Longitudinal follow up of small cohort of bicuspid and tricuspid patients. Those with bicuspid valve and abnormal flow patterns demonstrated significantly higher growth rates at follow-up. Those with eccentric flow demonstrated most rapid growth.

Lorenz et al. 2014[31]	28	4D flow CMR Helical flow EnSight, CEI, USA MATLAB (in-house), The Mathworks, USA	Helicity comparison between bicuspid patients and controls. Bicuspid patients demonstrated greater peak relative helicity during systole and greater heterogeneity in distribution of helicity in the aorta. Controls demonstrated consistent clockwise helicity in the ascending aorta (during peak and late systole) and counter clockwise in the descending aorta.
Mahadevia et al. 2014[18]	75	4D flow CMR Systolic flow angle, flow displacement, regional WSS EnSight, CEI, USA MATLAB (in-house), The Mathworks, USA	Blood flow patterns compared in bicuspid patients and matched controls. Eccentric outflow jet patterns in bicuspid patients led to elevated regional WSS at the right anterior wall for right-left fusion, and right-posterior wall for right-non fusion when compared to size matched controls. Type 1 and 3 aortopathy seen largely in right-non patients, and Type 2 in Right-left patients. Different aortopathy types demonstrated different degrees of flow displacement (Type 3 greatest, Type 1 least). Tricuspid valved patients with aneurysms demonstrated significantly decreased WSS compared to controls. Controls demonstrated centrally distributed peak systolic velocities, and less eccentric distribution of WSS.
Mirabella et al. 2015[25]	24	4D flow CMR Flow displacement, jet angle	Semi-automated protocol to assess geometry and haemodynamics in group of bicuspid patients and controls. Association found between aortic diameter and velocity (negative), jet angle (positive), and flow displacement (positive). Positive association between flow displacement and orifice jet angle in tricuspid subjects found. Bicuspid group had lower mean velocities in the proximal aorta, but significantly higher jet angle and flow eccentricity.

		OsiriX, Pixmeo, Switzerland MATLAB (in-house), The Mathworks, USA VMTK software Paraview, USA	
Raghav et al. 2018[27]	52	4D flow CMR Flow angle, flow displacement, jet quadrant OsiriX, Pixmeo, Switzerland MATLAB (in-house), The Mathworks, USA VMTK software Paraview, USA	Semi-automated protocol to assess haemodynamics in the ascending aorta in bicuspid aortic valve patients and tricuspid aortic valve controls. Right-non-coronary fusion bicuspid (RN-BAV) patients had greater association between proximal ascending aorta haemodynamics and distal ascending aorta diameter than right-left fusion bicuspid (RL-BAV) patients. Distal ascending aorta diameter was also found to correlate with upstream flow displacement and flow angle at the sino-tubular junction, with stronger correlation shown in RN-BAV patients than RL-BAV and tricuspid patients.
Schnell et al. 2016[35]	39	4D flow CMR Aortic shape, helix and vortex formation, peak velocities EnSight, CEI, USA	Comparison of relatives of bicuspid valve patients (with trileaflet valves) vs. controls. Cubic & gothic arches more prevalent in bicuspid relatives, as was vortex formation. Peak velocities were significantly lower in gothic vs. club aortas. Vortex flow was increased for cubic aortas in the proximal aorta and arch. Vortex and helix flows were elevated for gothic aortas in the proximal and descending aorta.

		MATLAB (in-house), The Mathworks, USA	
Shan et al. 2017[19]	65	4D flow CMR WSS, flow eccentricity EnSight, CEI, USA MATLAB (in-house), The Mathworks, USA	Comparison of flow patterns in bicuspid patients (right-left only) with aortic stenosis and regurgitation, compared with size matched controls. All bicuspid patients had peak WSS at the right-anterior portion of the ascending aorta (stenosis or regurgitance had no impact). Most patients had type 2 aortopathy, which was not influenced by valve dysfunction. The regurgitation group had universally elevated WSS in the ascending aorta, associated with elevated stroke volume. The stenosis group had elevated flow eccentricity, which correlated with increased peak valve velocity. The control patients with bicuspid valve had higher circumferentially averaged WSS than the tricuspid controls in the proximal aorta.
Sigovan et al. 2011[79]	41	4D flow CMR Flow eccentricity, jet angle, flow displacement EnSight, CEI, USA MATLAB (in-house), The Mathworks, USA	Relationship between flow eccentricity, jet angle, and flow displacement in a group of patients and controls. Jet flow angle and flow displacement were significantly higher in patients with mild eccentric systolic flow. In those with marked eccentric flow, only flow displacement was significantly elevated, suggesting it is a better characterisation than jet flow angle.
Van Ooij et al. 2015[20]	23	4D flow CMR WSS maps	Creation of patient-specific heat maps of WSS based on 4D flow MRI data based on averages and standard deviations calculated from volunteers. WSS was regionally higher in bicuspid patients (greater curvature of ascending aorta), which correlated with peak systolic velocity.

		Mimics, Materialise, Belgium MATLAB (in-house), The Mathworks, USA	
Van Ooij et al. 2016[80]	76	4D flow CMR WSS maps Mimics, Materialise, Belgium MATLAB (in-house), The Mathworks, USA	Investigation of age related changes in WSS and velocities in healthy controls and bicuspid patients. Significant inverse correlation found between age and peak systolic velocity and WSS, likely related to changes in aortic geometry, size, and compliance.
Von Knobelsdorff et al. 2016[81]	74	4D flow CMR WSS, helical and vortical flow, flow eccentricity, flow displacement, LV mass EnSight, CEI, USA MATLAB (in-house), The Mathworks, USA	Flow patterns and LV relative mass assessed in cohort of aortic stenotic patients and controls. Helical and vortical flow more prevalent in stenosis patients, which worsened with decreasing orifice area. Decreasing orifice area also associated with more eccentricity and flow displacement. Asymmetric and elevated WSS patterns more prevalent in patients. Bicuspid group showed more intense helical and vortcal flow, higher flow displacement, and higher peak systolic WSS. LV mass associated with aortic orifice area and flow displacement.
Youssefi et al. 2017[26]	45	2D PC- CMR and CFD	MRI and CFD used to assess flow patterns in a group of patients with stenotic or regurgitant valves (both bi- and tricuspid) compared to controls. Bicuspid group had greater eccentricity of flow. Helicity was greatest in those with Right-Non bicuspid

		WSS, OSI, helicity, flow eccentricity CRIMSON, Kings College, London MATLAB (in-house), The Mathworks, USA ParaView, Kitware, USA	valves. The greater curve of the aorta experienced highest WSS and lowest OSI in aortic stenosis patients. Aortic stenosis led to greater levels of WSS in the proximal aorta.

TABLE S3 – Thoracic aortic aneurysmal disease studies

Author & Year	Number of patients	Technique used, variables calculated, software used	Key findings / useful images
Barker et al. 2014[45]	42	4D flow CMR Laminar viscous energy loss Vmtk, Orobix, Italy ImageJ, NIH, USA	Assessment of impact of aortic dilatation on flow patterns. Viscous energy loss was significantly higher in patients with dilated thoracic aorta's and in those with aortic stenosis, when compared with healthy volunteers. The authors suggest that increased ventricular afterload may be related to abnormal flow and viscous energy loss, and that their technique allows this to be quantified and potentially used in the future as a clinical measure of risk stratification and aortic disease severity.
Bieging et al. 2011[36]	21	4D flow CMR WSS, streamlines, pathlines, helical & vertical flow MATLAB (in-house), The Mathworks, USA EnSight, CEI, USA	Assessment of impact of aortic dilatation on flow patterns. Time averaged WSS, and diastolic WSS was higher in patients with dilatation of the ascending aorta compared to controls. They also had decreased systolic to diastolic WSS ratio, delayed onset of peak WSS, and decreased peak systolic WSS. Maximal WSS was found to be on the anterior wall of the ascending aorta. Increased vertical and helical flow was also found during diastole.
Burk et al. 2012[37]	63	4D flow CMR WSS, OSI, helical & vertical flow, velocities	Assessment of impact of aortic dilatation on flow patterns. Patients with dilated ascending aortas had great incidence of helical and vertical flow in the ascending aorta. The strength of these corresponded to aortic diameter. Peak systolic WSS in the ascending aorta and arch was lower in patients with dilated aortas. Increasing aortic diameter was associated with increased

		EnSight, CEI, USA MATLAB (in-house), The Mathworks, USA	time to peak systolic velocity, OSI, and decreasing peak WSS. Peak systolic WSS was lowest in aneurysm patients at the right and outer curvature within the ascending aorta and arch.
Garcia et al. 2015[82]	40	4D flow CMR Segmental 3D velocity distribution MATLAB (in-house), The Mathworks, USA Mimics, Materialise, Belgium	Assessment of impact of aortic dilatation on flow patterns. With progressive aortic dilatation, there is more focal variation in peak systolic velocity throughout the aorta. Those with more severe dilatation were more likely to have increased aortic valve peak velocity, and more likely demonstrate localised outflow jets and high flow regions in the proximal aorta.
Geiger et al. 2012[40]	34	4D flow CMR Particle traces, streamlines, helical and vertical flow EnSight, CEI, USA	Comparison of Marfan patients and healthy volunteers. Local helix flow in the ascending aorta was significantly more common in patients with Marfan syndrome (without aneurysm or valve insufficiency) in comparison to healthy volunteers (with similar sized aortas). This increased with aortic diameter. Helix and vertical flow in the descending aorta was more common in Marfan patients.
Geiger et al. 2013[83]	36	4D flow CMR WSS, OSI	Comparison of Marfan patients and healthy volunteers. Patients with Marfan syndrome demonstrated lower peak systolic velocity, and higher circumferential WSS in the ascending aorta compared with healthy volunteers (similar sized aortas). They also demonstrated more WSS eccentricity, with higher WSS at the inner curvature of the proximal ascending aorta and at anterior

		EnSight, CEI, USA	part more distally. OSI was significantly lower in the descending aorta of Marfan patients.
Ha et al. 2017[39]	80	2D PC- CMR WSS, flow rates, flow skewness MATLAB, The Mathworks, USA	Assessment of patients with severe aortic stenosis to determine association of haemodynamic characteristics with aortic dilatation. Right posterior WSS was also significantly higher in the aortic dilatation group, with no other WSS parameters showing statistical difference. An ascending aorta diameter of >4cm showed significantly higher anterograde flow rates, retrograde flow, reverse flow fraction, and flow skewness at systole.
Harloff et al. 2010[84]	93	4D flow CMR WSS, OSI MATLAB (in-house), The Mathworks, USA EnSight, CEI, USA	Authors attempted to examine whether areas of aortic plaque were associated with the atherogenic pattern of low WSS and high OSI. No direct correlation was found except for in the region of the left anterior wall and the inner curvature of the proximal descending aorta.
Hope et al. 2007[42]	32	4D flow CMR Helical and retrograde flow patterns EnSight, CEI, USA Aspire2 (proprietary)	Comparison of flow patterns in aortic aneurysms vs. healthy volunteers. In healthy patients, classic pattern observed: right anterior skewed flow of blood in to ascending aorta which is reflected posterolaterally towards the inner curve creating opposing helices: a right-handed helix along the left wall, and a left-handed helix along the right wall. Retrograde flow occurs along the inner curve between the two helices. In the descending aorta, flow forms a clockwise helix. In patients with aneurysms, larger helices were observed, and retrograde flow occurred earlier and for a longer period. In healthy patients, the velocity between the ascending aorta and the arch decreased, whereas it increased

			in aneurysm patients. However, overall no apparent correlation between pathology and flow pattern could be seen, and no relationship between diameter of aneurysm and type of flow pattern.
Kari et al. 2015[85]	31	4D flow CMR Flow compression index (fraction of the area of high velocity mid-systolic flow over cross-sectional area) – lower value means more flow compression EnSight, CEI, USA UTHCSA Image Tool Software, UTHCSA, USA	Assessment of aneurysm morphology on levels of flow compression in aorta. High levels of flow compression or 'peripheralisation' were seen in patients with eccentric aneurysm morphology (i.e. normal root with enlargement above the sinotubular junction). Low levels were seen in those with non-eccentric aneurysms with diffuse and tubular enlargement. Type of valve dysfunction not predictive for flow compression.
Van Ooij et al. 2015[20]	30	4D flow CMR WSS, cohort-averaged systolic WSS MATLAB (in-house), The Mathworks, USA Mimics, Materialise, Belgium	Cohort-averaged systolic WSS calculated for a group of volunteers, aneurysm and aortic stenosis patients. Patients with aortic dilatation showed significantly lower WSS on 7% of the ascending aorta (distal outer curvature and proximal inner curvature), and stenosis patients showed significantly higher WSS on 34% of the ascending aorta (entire outer curvature). Purpose of study was to show feasibility of generating cohort-averaged WSS maps.

		Linear Image Registration Tool (FLIRT), FMRIB	
Von Spiczak et al. 2015[43]	13	4D flow CMR Vortex quantification GTFlow, GyroTools, Switzerland In-house C++ tool built within above software Eigen, TuxFamily.org Coin3D, Coin3D.org	Quantitive method of assessing vortex formation used on group of volunteers and aneurysm patients. Patients demonstrated helical flow early in the ascending aorta which peaked in mid-systole in the arch. 3D vortex cores (right handed) escalated in early systole, peaking in mid systole. In those with aneurysms, vortex flow developed late in mid/end-systole close to the aortic bulb, and no physiological helix seen in the arch. Degree of vortical flow increased with aneurysm size.
Wang et al. 2016[41]	32	4D flow CMR WSS, OSI, nonroundness (measure of asymmetry of segmental WSS), Vorticity, helicity MATLAB (in-house), The Mathworks, USA EnSight, CEI, USA	Comparison of Marfan patients and healthy volunteers. Marfan patients had lower axial WSS in the root and lower circumferential WSS in the arch compared to healthy patients. They also demonstrated higher OSI (axial and circumferential) at the sinotubular junction and arch, but lower OSI (circumferential) in the descending aorta. Marfan patients demonstrated significantly more asymmetry in segmental WSS patterns. WSS was strongly correlated with body surface area and aortic size in Marfan patients. In this study aortic diameter was not similar in the Marfan and healthy groups. The Marfan group had lower flow velocity during systole, and smaller vorticity and helicity than the healthy group (especially in the proximal aorta).

Weigang et al. 2008[44]	7	4D flow CMR 3D streamlines, particle traces. EnSight, CEI, USA MATLAB (in-house), The Mathworks, USA	Assessment of impact of aortic dilatation on flow patterns. Classical right handed helical flow extending in to the arch seen in healthy patients. Minimal vortical flow seen in the sinuses. In aneurysmal patients, this right-handed helix was more pronounced with flow acceleration along the greater curvature, or with multiple vortical flows in the sinuses and middle of the ascending aorta.

TABLE S4 – Aortic coarctation

Author & Year	Number of patients	Technique used, variables calculated, software used	Key findings / useful images
Andersson et al. 2015[50]	6 coarctation treatment simulations based on 1 patients data	2D PC- CMR and CFD (Large eddy simulation) Turbulent kinetic energy, flow eccentricity Segment, Heiberg ANSYS Mechanical, CFX and ICEM, Ansys Inc, USA	Haemodynamic parameters assessed with CFD in a pre-treated aortic coarcation patient, and after several virtual interventions to indicate impact of different dilatation options. Inverse relationship between turbulent kinetic energy and degree of dilatation of the stenosis found. Greater dilatation also led to less flow eccentricity. However, the total amount of turbulence did not decrease any further following 30% of stenotic dilatation. In addition, flow condition improvements were seen in eccentric dilatation of the lesion rather than concentric.
Frydrychowicz et al. 2011[46]	47	4D flow CMR Helicity, WSS, OSI, peak velocities EnSight, CEI, USA MATLAB (in-house), The Mathworks, USA	This paper characterised haemodynamic flow in patients with and without repair of coarctation, compared with healthy volunteers (similar sized aortas). Volunteers and patients demonstrated the same amount of overall aortic helicity, but the number of additional localised helix or vortex was significantly higher in patients. Vortices in the orifices of the head and neck vessels (especially left subclavian) were detected in significantly more patients. WSS (overall magnetitude) was significantly higher in patients, with a lower overall OSI. In summary, alterations in haemodynamics (in particular secondary flow patterns) in coarctation patients (post repair) are not limited to the specific region of repair, but found in the entire aorta.
Hope et al. 2010[47]	42	4D flow CMR	Comparison of coarctation patients (before and after repair) vs healthy. Coarctation patients demonstrated abnormal blood flow

		Helical and vortical flow, 3D streamlines and particle traces, velocities EnSight, CEI, USA Aspire2, Stanford, USA	patterns in the descending thoracic aorta: helical flow post repair, vortical flow in regions of post stenotic dilatation, and abnormal geometric angulation of the aorta in some post repair patients which was possibly related to the degree of helical flow in the descending thoracic aorta.
LaDisa et al. 2011[48]	6	2D PC- CMR and CFD Velocity, WSS, OSI (both longitudinal and circumferential) SimVascular/ParaView, Kitware, USA	CFD performed on cohort of coarctation patients post repair (end-to-end) and age matched controls. The overall distal aorta exposed to subnormal TAWSS and OSI was similar in patients and controls, but several local differences existed – controls had left handed rotating patterns of TAWSS and OSI down the descending thoracic aorta, and TAWSS was higher in coarctation patients near the site of residual narrowing. OSI was also higher distally in patients, especially along the left distal aortic wall. Vortices were observed in several of the coarctation patients in the region of the repair.
LaDisa et al. 2011[49]	5	2D PC- CMR and CFD Vessel deformation, ascular resistance, compliance, OSI, WSS, cyclic strain SimVascular/ParaView, Kitware, USA	CFD simulation in coarctation patients (variety pre and post repair) and a volunteer, where simulation replicated normal resting blood flow and that during exercise. Greater exercise induced changes in coarctation patients . Cyclic strain elevated in the proximal aorta for coarctation patients, which reduced post treatment. Coarctation patients had a greater proportion of aorta exposed to abnormal WSS or elevated OSI.

Taelman et al. 2016[86]	4 simulations based on 1 patients data	2D PC- CMR and CFD (FSI) Pressure, vortices Mimics, Materialise OsiriX Ansys Fluent Simulia Abaqus	A numerical FSI model was created to predict central haemodynamics in coarctation treatment. Residual narrowing in coarctation significantly affected the simulations haemodynamics, where a short segment can cause very significant increases in blood pressure, which is attributed to both the narrowing and the stiffness of the segment. In longer segments of coarctation, stiffness contributes less to increases in blood pressure relative to the length of the coarctation. Downstream vortices, swirling and flow instability seen as blood crosses the coarctation region. These changes are mainly attributable to the stenosis rather than stiffness of the coarctation segment.

TABLE S5 – Aortic dissection patients

Author & Year	Number of patients	Technique used, variables calculated, software used	Key findings / useful images
Dillon-Murphy et al. 2016[51]	3 simulations from 1 patients data	2D PC- CMR and 4D flow CMR and CFD CRIMSON (in-house)	Assessment of haemodynamics in a dissection patient with CFD. Local regions of increased velocity, pressure, WSS, and flow alterations were noted, especially in the narrow true lumen and around the primary dissection tear. Estimated 14% increase in ventricular work with the onset of dissection. When the presence of secondary tears was modelled as being excluded, increase in flow and pressure drop in true lumen.
Francois et al. 2013[54]	12	4D flow CMR Streamlines, particle traces, helicity, Net flow, retrograde flow, peak flow, time to peak MATLAB (in-house), The Mathworks, USA EnSight, CEI, USA	Flow assessment in the true and false lumens of dissection patients (mixture of type A/B and operated/unoperated. In general, slower flow was seen in false lumens, which demonstrated complex abnormal flow patterns. Systolic retrograde flow visualised in both lumens, which was often vortical and occurred more frequently in the false lumen. Retrograde flow often occurred earlier in the false lumen.
Karmonik et al. 2010[55]	Pre- and post intervention simulations from 1 patients	2D PC- CMR and CFD WSS, Pressure, velocity Fluent, Ansys Inc, USA	Patient specific CFD simulations conducted to assess haemodynamics in type B dissection pre- and post-treatment. Pre-treatment, large WSS and dynamic pressure noted at entrance of the tear and a stenotic region in the true lumen. Post treatment, this improved significantly, except at the proximal end of the stent graft and at the re-entrance tear. Two focal

			regions of high dynamic pressure within the stent graft. Only slow retrograde flow present in false lumen post treatment
Karmonik et al. 2012[52]	1 with longitudinal follow-up	2D PC- CMR and CFD WSS, Pressure, velocity Fluent, Ansys Inc, USA	MRI and CFD to assess blood flow in a patient with an enlarging type B dissection. High velocity prounced jet in to entry tear from true lumen, with a slow flow zone with recirculation adjacent to false lumen wall. Dilatation of the false lumen at follow-up demonstrated changes in velocity, pressure and WSS (all lower).
Karmonik et al. 2013[87]	2	2D PC- CMR and CFD WSS, Pressure, velocity Fluent, Ansys Inc, USA MATLAB (in-house), The Mathworks, USA Paraview, Kitwork, USA	Comparison of flow patterns in type B dissection and healthy aorta using CFD. WSS lower in region of dilatation compared to healthy aorta. Higher pressure gradient between ascending and descending aorta in dissection patient.
Strotzer et al. 2000[53]	14	2D PC- CMR Flow rates, retrograde flow	Assessment of flow patterns in the true and false lumen of aortic dissection. Lower volume flow, velocity, and average peak velocity in the false lumens. Most false lumens showed bidirectional flow, compare to just a single patient with bidirectional flow in the true lumen. Significantly more flow irregularity seen in the false lumen.

TABLE S6 – Aortic prosthesis insertion

Author & Year	Number of patients	Technique used, variables calculated, software used	Key findings / useful images
Bogren et al. 2000[67]	12	4D flow CMR Flow streamlines, particle paths, vortex and helix formation MRI View (custom)	Assessment of blood flow patterns in thoracic aortic grafts (ascending & descending aorta) inserted for a number of different pathologies. In all patients, acceleration and jet formation was seen in to and/or out of the grafts. Vortices were observed proximally, in, or distal to the graft. Those with underlying atherosclerosis had the most abnormal flow with multiple vortices in and outside of the graft. Blood persisted up to one and a half heart beats in some vortices, and 3-5 heartbeats to flow from ascending to descending compared with the age matched controls. Energy loss due to the grafts were estimated at up to 33%.
Bollache et al. 2017[73]	53	4D flow CMR WSS MATLAB (in-house), The Mathworks, USA	Comparison of WSS indices pre- and post-surgery in 33 patients with aortopathy to determine impact of different proximal aorta interventions on WSS indices. A further 20 no-surgery aortopathy patients were included to determine changes in WSS indices on follow-up. WSS indices were stable in controls over time. Proximal aortic WSS decreased after aortic valve replacement, but WSS increased in areas distal to graft after aortic root replacement.
Cheng et al. 2015[63]	6	2D PC CMR & CFD Mimics, Materialise, Belgium	CFD analysis of blood flow in a cohort following composite bioprosthetic root replacement. Following insertion of the graft the vortical flow structure and haemodynamic parameters in the aorta were altered: slightly reduced helical flow index, elevated wall shear stress in the ascending and arch, decreased WSS in the descending aorta, and greater non-uniformity in wall

		MATLAB (in-house), The Mathworks, USA ANSYS, Ansys Inc, USA Turtuosity, Outflow angle, WSS, OSI, SRI, Helical flow index	shear compared to normal patients. Highest levels of WSS were seen at branch points in controls and at the distal anastomosis in patients. Geometrical differences between patients and controls (tortuosity and aortic angle) were noted, which in addition to the material properties of the dacron, may account for some of the haemodynamic changes. The geometry seemed to account for the direction of jetflow from the aortic valve.
Collins et al. 2015[68]	37	4D flow CMR 3D pathlines and streamlines, helical flow, velocities, flow profile uniformity MATLAB (in-house), The Mathworks, USA EnSight, CEI, USA	Comparison of flow patterns in controls, and patients who had root replacement with either a composite biological prosthesis or valve sparing procedure. Peak velocity was higher in root replacements compared to controls, except in the descending aorta where the valve sparing root group only had greater velocities. Composite root replacement patients had higher flow asymmetry and increased helical flow (not particularly pronounced) compared to valve sparing roots. Overall suggestion of superior haemodynamics in valve sparing patients.
Frydrychowicz et al. 2009[70]	13	4D flow CMR 3D streamlines and particle traces, helicity, vorticity MATLAB (in-house), The Mathworks, USA	Assessment of flow patterns in a patient post valve sparing root (David 1) compared to group of age matched controls. Smooth blood flow seen through the graft, with a right handed helical flow observed, and no flow accelerations. Helicity was more pronounced than in controls, but flow jets or vortices not seen. Physiological retrograde flow (largely at inner curve of ascending aorta) and vortices observed in controls, but not in root replacement patient, possibly due to longer period of systole or decreased compliance of the graft.

		EnSight, CEI, USA	
Hellmeier et al. 2017[60]	10	CFD WSS, secondary flow degree, transvalvular pressure drop, turbulent kinetic energy, normalised flow displacement ZIBAmira, Zuse Institute Berlin, Berlin, Germany Gambit, Ansys, Canonsburg, USA ReMESH, IMATI, Genoa, Italy SolidWorks, Dessault Systemes SolidWorks Corp., Waltham, USA	Determine the haemodynamic impact of mechanical (Regent valve, St. Jude Medical, Saint Paul, USA) versus biological (Fisics-Incor valve, INCOR, Sao Paulo, Brazil) aortic valve prostheses. Biological prostheses resulted in higher WSS and secondary flow degree in the ascending aorta, and greater transvalvular pressure drop and turbulent kinetic energy than the mechanical prostheses. Great interpatient variability was observed, suggesting need for patient-specific evaluation.
Hope et al. 2013[88]	17	4D flow CMR Flow streamlines, WSS, flow	Assessment of flow conditions in Marfan patients post valve sparing root replacement compared to healthy controls. One of the Marfan patients developed a type B dissection (near the distal anastomosis) during follow-up after his scan. His scan prior to this demonstrated altered flow patterns, increased WSS along the anterior right ascending aorta (and decreased along the inner curve), and increased flow displacement in

		displacement/eccentricity (all during peak systole) MATLAB (in-house), The Mathworks, USA EnSight, CEI, USA Aspire2, Stanford, USA	comparison to the rest of the post-operative cohort who did not develop complications. In the rest of the cohort, laminar flow was seen throughout the aorta during peak systole. In half, a small helix was visible at the inner curve of the descending aorta. Two patients demonstrated vortical flow in the proximal descending aorta, one of whom developed the Type B dissection.
Keller et al. 2016[61]	20	4D flow CMR Vortex/helix formation, pressure gradients MATLAB (in-house), The Mathworks, USA Mimics, Materialise, Belgium EnSight, CEI, USA	Pre and post op assessment (in same patients) of flow patterns following root replacement with a mechanical valved conduit (On-X). Comparison group of matched controls. Highly helical and vortical flow in all patients pre-operatively, which reduced significantly after surgery, restoring patterns similar to controls. Peak transvalvular pressure gradients reduced after surgery but were still not comparable to controls.
Konoura et al. 2013[89]	3 patients with 4 simulations	2D PC- CMR and CFD Blood flow distribution MATLAB (in-house), The Mathworks, USA ANSYS, Ansys Inc, USA	MRI and CFD used to simulate blood flow distribution in to the head and neck vessels in either 3 or 4 branch grafts used for arch replacement. Blood flow distribution was found to be similar for both grafts, suggesting the newly developed 3 branch grafts are acceptable in terms of blood flow distribution.

Kozerke et al. 2001[58]	6	4D flow CMR Particle paths, animated velocity vector plots Home built software made with Visual C++	Flow pattern in patients with mechanical aortic valves (all St Jude) assessed. Distinct flow pattern reflecting the valve design was seen closest to the valve during early flow acceleration (two lateral jets corresponding to the orifices), with reverse flow and vortices occuring next to high velocity jets and above the hinge housings. During later systolic flow became confined to the central vessel area, with peak velocities directed to the outer curve and reverse flow along the inner aortic curvature. Further downstream, more variability in flow patterns depending on patients anatomy.
Kvitting et al. 2004[72]	8	4D flow CMR Velocity EnSight, CEI, USA	Flow pattern in Marfan patients post valve sparing root (straight tube with no sinuses) compared to healthy controls. In normal patients, vortical flow visible in sinuses after peak systole in to diastole, which persisted until diastole. Vortices larger over right and non-coronary sinuses. No such vortices observed in Marfan patients who had straight Dacron grafts. Otherwise, similar velocity, duration of systolic flow, and time to peak for both groups.
Leuprecht et al. 2003[59]	2	2D PC- CMR and CFD WSS, velocity profiles	Comparison of flow patterns in a healthy volunteer and a patient following aortic valve replacement (St Jude mechanical). Several differences seen: the flow profile in the ascending aorta and arch of the valved patient corresponded to the two orifices of the valve. WSS was significantly higher, due to higher flow acceleration which was asymmetric causing regionally higher WSS at specific points.
Liu et al. 2009[90]	35	4D flow CMR Turbulence, vortical flow	Flow patterns assessed in a cohort of patients post valve sparing root replacement, those with aneurysms and healthy volunteers. The valve sparing root group had similar levels of turbulence to the control group. The aneurysm group had significantly greater turbulence. Presence of vortices in the

		4D Flow, Siemens Medical	sinuses of Valsalva was similar between valve-sparing and control groups. Vortices were significantly reduced in the aneurysm group compared to the control group.
Markl et al. 2005[71]	22	4D flow CMR Particle traces, velocity vector fields, vortex and helix formation EnSight, CEI, USA	Comparison of flow in patients post valve sparing root (David) and healthy controls. Vortices seen in the sinuses of all controls (greatest in the left, then the right, and least in the non coronary sinus). Comparable vortices seen in all operated patients regardless of neosinus creation, except for the David-V group which had greater vortex formation over the non-coronary cusp. Retrograde flow (late systolic and early diastolic) and helix formation in the ascending aorta was significantly higher in the operated patients.
Midulla et al. 2012[64]	40	2D PC-CMR and CFD 3D streamlines, Velocity mapping, WSS Amira, Mercury Computer Systems, USA AVBP Solver, European Centre for Research and Advanced Training in Scientific Computation	Cohort of patients underwent MRI and CFD post TEVAR (Gore and Medtronic), compared with controls. Regions of high WSS and velocity noted at the ends of the stented segments in a number of patients.
Oechtering et al. 2016[65]	30	4D flow CMR Streamlines, particle traces, vortices, pressure	Comparison of flow patterns in those post valve sparing root (sinus shaped Uni-Graft) and matched controls. The valve sparing patients had significantly larger vortices (of similar configuration – i.e. starting in early systole, peaking after peak systole) compared to controls. Similar peak transvalvular

		differences, transvalvular pressure gradient GTFlow, GyroTools, Switzerland	pressure gradients. Overall closely matched haemodynamics between the groups, except the deceleration phase of decreasing pressure gradient at the end of systole, which was longer in the valve sparing group.
Semaan et al. 2014[66]	33	4D flow CMR 3D pathlines, helical flow, flow uniformity, velocities, retrograde flow. EnSight, CEI, USA	Assessment of haemodynamic conditions post valve sparing root compared with matched pre-surgical controls (i.e. those awaiting surgery with pathology). Pronounced helical flow in presurgical candidates compared to postoperative group. Presurgical flow was more eccentric for bicuspid valve patients compared to tricuspid. Eccentricity reduced in post-op patients. Peak velocities were higher in the post-op group (especially in the right anterior quadrant), more so in bicuspid valve patients, especially in the ascending aorta.
Singh et al. 2015[74], Singh et al. 2016[75], and Singh et al. 2016[76]	3	2D PC- CMR and CFD Peak stress, displacement, helical flow index, flow rate, WSS Mimics, Materialise, Belgium MATLAB (in-house), The Mathworks, USA ANSYS, Ansys Inc, USA	Pre-and post op MRI and CFD used to assess the impact of aortic root surgery on Marfan patients using a personalised external aortic support (PEARS). Post implantation, little change in geometry of patient aorta. However, before PEARS implantation, peak stresses, displacements were located at the sinuses of Valsalva, but following surgery, these were shifted to the aortic arch, especially at the region between supported and unsupported aorta. There was a significant reduction in systolic downward motion of the aortic root (axial displacement) following PEARS implantation. Despite the above, only minor changes in helical flow index and WSS patterns post implantation.

Stephens et al. 2015[91]	24	4D flow CMR WSS, flow eccentricity, helical flow MATLAB (in-house), The Mathworks, USA EnSight, CEI, USA	Asessment of the influence of bicuspid valve type on flow patterns following valve sparing root. Control group of tricuspid valves. Most patients had helix formation in the ascending aorta, usually a single right handed one, but sometimes two countervailing helices (the right handed being larger). A single patient with a type B dissection had a large region of vortical flow in the proximal descending aorta. Both average magnitude and ratio of WSS (along outer curve to inner curve) greater in Sievers' type 1 (Left-Right fusion, which has systolic flow oriented towards the outer curve) compared to Sievers' type 0 in the proximal aorta. Type 1, but not Type 0 had higher WSS ratio compared to tricuspid patients. No differences found in flow eccentricity, despite the cusp angle of the Type 1 being significantly lower than Type 0.
Tan et al. 2012[56]	1 (pre- and post simluations)	2D PC- CMR and CFD WSS, OSI, turbulence, velocities, turbulent kinetic energy Mimics, Materialise, Belgium MATLAB (in-house), The Mathworks, USA ANSYS, Ansys Inc, USA	MRI and CFD pre and post transcatheter aortic valve implantation (Medtronic CoreValve). Prior to the procedure, highly disturbed turbulent flow and jet impacting the wall of the arch due to the impaired opening of the stenotic aortic valve. Post procedure, velocity profile more similar to healthy aorta, with spatially uniform WSS and lower turbulence.

Torii et al. 2012[69]	44	2D PC- CMR Spatiotemporal velocity and flow plots, shear rate, outflow area The Mathworks, USA	Spatiotemporal velocity distribution assessment at multiple aortic locations in multiple patients who had undergone various types of root intervention, compared with a group of controls. Intervention patients tended to have higher velocities than the control group and autograft group (which had a relatively balanced profile), especially with xenografts, which also had steeper velocity profiles with higher peaks. Main conclusion from this paper is different root substitutes have very different flow patterns.
Trauzeddel et al. 2016[57]	38	4D flow CMR Vortical and helical flow, flow eccentricity, WSS MATLAB (in-house), The Mathworks, USA EnSight, CEI, USA	Comparison of flow patterns in groups who had undergone aortic valve replacement with either transcathether technique (Edwards SAPIEN XT) or conventional open (stented bioprosthesis) surgery. Compared to a group of healthy subjects. The conventional open group had more extensive vortical and helical flow pattern than the transcathether and control groups. The transcathether group had more extensive voritcal flow than controls. Both surgical groups had marked flow eccentricity and asymmetric WSS distribution (max at the left posterior wall) vs. controls.
Van Kesteren et al. 2017[62]	28	4D flow CMR Flow velocity, WSS, viscous energy loss (all during peak systole) MATLAB, The Mathworks, USA	Evaluate differences in haemodynamic parameter between stented and stentless aortic valve bioprostheses 1-year post-replacement. No significant differences were shown for peak and mean flow velocity, but there was higher central lumen velocity, and lower outer lumen velocity, WSS, and viscous energy loss for stentless bioprostheses.

		Mimics, Materialise, Belgium	
Von Knobelsdorff-Brenkenhoff et al. 2014[81]	47	4D flow CMR Vortex and helix flow, systolic flow eccentricity, WSS MATLAB (in-house), The Mathworks, USA EnSight, CEI, USA	Assessment of blood flow patterns in the ascending aorta following conventional aortic valve replacement (multiple types including mechanical, stentless and autograft root), compared to healthy controls. Compared to controls, those with mechanical valves showed the most vorticity, and those with stented bioprosthesis the most helicity. All patients (apart from autograft group) had evidence of eccentric flow jets, mainly directed towards the right anterior aortic wall. This often led to eccentric WSS patterns, especially in those with stented and stentless valves. Autografts exhibited lower peak WSS than controls. Controls did not have eccentric flow.

Additional References

78. Garcia J, Barker AJ, Murphy I, Jarvis K, Schnell S, Collins JD, Carr JC, Malaisrie SC and Markl M. Four-dimensional flow magnetic resonance imaging-based characterization of aortic morphometry and haemodynamics: impact of age, aortic diameter, and valve morphology. *Eur Heart J Cardiovasc Imaging*. 2016;17:877-84.

79. Sigovan M, Hope MD, Dyverfeldt P and Saloner D. Comparison of four-dimensional flow parameters for quantification of flow eccentricity in the ascending aorta. *J Magn Reson Imaging*. 2011;34:1226-30.

80. van Ooij P, Garcia J, Potters WV, Malaisrie SC, Collins JD, Carr JC, Markl M and Barker AJ. Age-related changes in aortic 3D blood flow velocities and wall shear stress: Implications for the identification of altered hemodynamics in patients with aortic valve disease. *J Magn Reson Imaging*. 2016;43:1239-49.

81. von Knobelsdorff-Brenkenhoff F, Trauzeddel RF, Barker AJ, Gruettner H, Markl M and Schulz-Menger J. Blood flow characteristics in the ascending aorta after aortic valve replacement--a pilot study using 4D-flow MRI. *Int J Cardiol*. 2014;170:426-33.

82. Garcia J, Barker AJ, van Ooij P, Schnell S, Puthumana J, Bonow RO, Collins JD, Carr JC and Markl M. Assessment of altered three-dimensional blood characteristics in aortic disease by velocity distribution analysis. *Magn Reson Med*. 2015;74:817-25.

83. Geiger J, Arnold R, Herzer L, Hirtler D, Stankovic Z, Russe M, Langer M and Markl M. Aortic wall shear stress in Marfan syndrome. *Magn Reson Med*. 2013;70:1137-44.

84. Harloff A, Nussbaumer A, Bauer S, Stalder AF, Frydrychowicz A, Weiller C, Hennig J and Markl M. In vivo assessment of wall shear stress in the atherosclerotic aorta using flow-sensitive 4D MRI. *Magn Reson Med*. 2010;63:1529-36.

85. Kari FA, Kocher N, Beyersdorf F, Tscheuschler A, Meffert P, Rylski B, Siepe M, Russe MF and Hope MD. Four-dimensional magnetic resonance imaging-derived ascending aortic flow eccentricity and flow compression are linked to aneurysm morphologydagger. *Interact Cardiovasc Thorac Surg*. 2015;20:582-7; discussion 587-8.

86. Taelman L, Bols J, Degroote J, Muthurangu V, Panzer J, Vierendeels J and Segers P. Differential impact of local stiffening and narrowing on hemodynamics in repaired aortic coarctation: an FSI study. *Med Biol Eng Comput*. 2016;54:497-510.

87. Karmonik C, Muller-Eschner M, Partovi S, Geisbusch P, Ganten MK, Bismuth J, Davies MG, Bockler D, Loebe M, Lumsden AB and von Tengg-Kobligk H. Computational fluid dynamics investigation of chronic aortic dissection hemodynamics versus normal aorta. *Vasc Endovascular Surg*. 2013;47:625-31.

88. Hope TA, Kvitting JP, Hope MD, Miller DC, Markl M and Herfkens RJ. Evaluation of Marfan patients status post valve-sparing aortic root replacement with 4D flow. *Magn Reson Imaging*. 2013;31:1479-84.

89. Konoura C, Yagi T, Nakamura M, Iwasaki K, Qian Y, Okuda S, Yoshitake A, Shimizu H, Yozu R and Umezu M. Numerical analysis of blood flow distribution in 4- and 3-branch vascular grafts. *J Artif Organs*. 2013;16:157-63.

90. Liu X, Weale P, Reiter G, Kino A, Dill K, Gleason T, Carroll T and Carr J. Breathhold time-resolved three-directional MR velocity mapping of aortic flow in patients after aortic valve-sparing surgery. *J Magn Reson Imaging*. 2009;29:569-75.

91. Stephens EH, Hope TA, Kari FA, Kvitting JP, Liang DH, Herfkens RJ and Miller DC. Greater asymmetric wall shear stress in Sievers' type 1/LR compared with 0/LAT bicuspid aortic valves after valve-sparing aortic root replacement. *J Thorac Cardiovasc Surg*. 2015;150:59-68.